JCI insight

BRD7 as key factor in PBAF complex assembly and CD8$^+$ T cell differentiation

Feng Huang, … , Hui Zhang, Bingfeng Liu

JCI Insight. 2024. https://doi.org/10.1172/jci.insight.171605.

Research In-Press Preview **Immunology** **Infectious disease**

Upon infection, naïve CD8$^+$ T cells differentiate into cytotoxic effector cells to eliminate the pathogen-infected cells. Although many mechanisms underlying this process have been demonstrated, the regulatory role of chromatin remodel system in this process remains largely unknown. Here we showed that BRD7, a component of the polybromo-associated BRG1-associated factor complex (PBAF), was required for naïve CD8$^+$ T cells to differentiate into functional short-lived effector cells (SLECs) in response to acute infections caused by influenza virus or lymphocytic choriomeningitis virus (LCMV). BRD7-deficiency in CD8$^+$ T cells resulted in profound defects in effector population and functions, thereby impairing viral clearance and host recovery. Further mechanical studies indicated that the expression of BRD7 significantly turned to high from naïve CD8+ T cells to effector cells, bridged BRG1 and PBRM1 to the core module of PBAF complex, consequently facilitating the assembly of PBAF complex rather than BAF complex in the effector cells. The PBAF complex changed the chromatin accessibility at the loci of *Tbx21* gene and up-regulated its expression, leading to the maturation of effector T cells. Our research confirms BRD7 and the PBAF complex are key in CD8$^+$ T cell development and present a significant target for advancing immune therapies.

BRD7 as Key Factor in PBAF Complex Assembly and CD8$^+$ T Cell Differentiation

Feng Huang[1,2#], Yingtong Lin[1,3#], Yidan Qiao[1#], Yaochang Yuan[1#], Zhihan Zhong[1], Baohong Luo[1], Yating Wu[4], Jun Liu[3], Jingliang Chen[5], Wanying Zhang[1], Hui Zhang[1], and Bingfeng Liu [1*]

1. Institute of Human Virology, Key Laboratory of Tropical Disease Control of Ministry of Education, Guangdong Engineering Research Center for Antimicrobial Agent and Immunotechnology, Zhongshan School of Medicine, Sun Yat-sen University, Guangzhou, Guangdong, China.
2. Guangzhou Laboratory, Guangzhou, China.
3. Guangdong Provincial People's Hospital, Guangdong Academy of Medical Sciences, Guangzhou, Guangdong, China.
4. The first Clinical Medical College, Southern Medical University, Guangzhou, China.
5. Infectious Diseases Center, Guangzhou Eighth People's Hospital, Guangzhou Medical University, Guangzhou, China.

# These authors contributed equally to this work.

*Corresponding author. Email: liubf5@mail.sysu.edu.cn, Tel: +86-20-87332588Sun Yat-Sen University, No. 74, 2nd Zhongshan Road, Guangzhou, Guangdong Province, 510080, PRC

Running title:
BRD7 Facilitates the Differentiation of Effector CD8$^+$ T cells

Keywords: BRD7, SWI/SNF, PBAF Complex, CD8$^+$ T cell Differentiation, Viral Infection

ABSTRACT

Upon infection, naïve $CD8^+$ T cells differentiate into cytotoxic effector cells to eliminate the pathogen-infected cells. Although many mechanisms underlying this process have been demonstrated, the regulatory role of chromatin remodel system in this process remains largely unknown. Here we showed that BRD7, a component of the polybromo-associated BRG1-associated factor complex (PBAF), was required for naïve $CD8^+$ T cells to differentiate into functional short-lived effector cells (SLECs) in response to acute infections caused by influenza virus or lymphocytic choriomeningitis virus (LCMV). BRD7-deficiency in $CD8^+$ T cells resulted in profound defects in effector population and functions, thereby impairing viral clearance and host recovery. Further mechanical studies indicated that the expression of BRD7 significantly turned to high from naïve $CD8^+$ T cells to effector cells, bridged BRG1 and PBRM1 to the core module of PBAF complex, consequently facilitating the assembly of PBAF complex rather than BAF complex in the effector cells. The PBAF complex changed the chromatin accessibility at the loci of *Tbx21* gene and up-regulated its expression, leading to the maturation of effector T cells. Our research confirms BRD7 and the PBAF complex are key in $CD8^+$ T cell development and present a significant target for advancing immune therapies.

INTRODUCTION

$CD8^+$ T cells play critical roles in protective immunity against intracellular pathogens including viruses. In response to viral infection, naive $CD8^+$ T cells rapidly undergo a pronounced clonal expansion and differentiate into antigen-specific effector cells to eliminate infected cells (1, 2). During this process, effector $CD8^+$ T cells acquire the ability to produce cytolytic and effector cytokines such as granzyme B (Gzmb) and interferon gamma (IFN-γ) (2-4). Within the effector populations, many effector $CD8^+$ T cells are short-lived effector cells (SLECs) which undergo programmed cell death, leaving behind a small population of memory precursor effector cells (MPECs) (5). These two subsets are divided by two critical surface markers, KLRG1 and IL7R (CD127). SLECs express high levels of KLRG1 and low levels of IL7R and exhibit higher expression of effector molecules, while MPECs express high levels of IL7R and low levels of KLRG1 and show a greater stem-cell like properties. The clonal expansion and effector differentiation of $CD8^+$ T cells are regulated by various transcription factors. Several transcription factors including T-bet, Blimp-1, Id2, and IRF4 are critical regulators for the differentiation of SLECs population (5-9), while Eomes, Foxo1, Id3 and Tcf1 are required for the differentiation of MPEC population (8, 10-13). The epigenetic and chromatin states also influence the differentiation of SLECs and MPECs (14, 15). However, more epigenetic mechanisms by which SLECs become committed to a terminal fate remain to be elucidated.

SWItch/Sucrose Non-Fermentable (SWI/SNF) chromatin-remodeling complexes contain members of ATPases that regulate DNA-protein contacts through energy generated from ATP hydrolysis. These ATP-dependent chromatin remodeling complexes are multimeric molecular assemblies involved in the regulation of chromatin architecture (16-19). Previous studies revealed that SWI/SNF complexes in mammalian cells exist in three non-redundant assembly bodies: BRG1/BRM-associated factor complex (BAF), polybromo-associated BAF complex (PBAF), and non-canonical BAF complex (ncBAF) (17). SWI/SNF complexes include many core components (20). Among them, SMARCB1, SMARCC1, SMARCC2, SMARCD1, and SMARCE1 are the components of “core module”, while BRG1 (or named as SMARCA4) belong to the ATPase module of the complexes. All of these modules are shared by both BAF and PBAF complexes.

Besides its important role in cancers, BRG1 is also important for T cell differentiation since BRG1 deficiency in mice results in thymic abnormalities and a developmental block at double negative to double positive T cell transition (21, 22). The specific components of BAF complex include ARID1A, ARID1B, and DPF2, while the specific components of PBAF complex include Bromodomain-containing protein 7 (BRD7), PBRM1, PHF10, and ARID2 (17, 20, 23, 24). It remains to be determined how the ATPase module and the BAF core module are assembled together and what is the role played by these special components.

BRD7 belongs to the bromodomain family, and can recognize and bind to acetylated histone H (25-27). It is ubiquitously expressed in the nucleus and only belongs to PBAF complex (25, 28). BRD7 has been reported as a transcriptional regulator and plays a critical role in cellular growth, cell cycle progression, and tumor development (28-36). Along with its PBAF partners, BRD7 participates in in β cells regulation or the resistance of tumor cells to immune cells (37, 38). Depletion of these genes in tumor cells would enhance the secretion of various chemokines which help recruit effector T cells (38). Although the interactions among components within PBAF complex has been largely determined in a recent biochemical study (17), it remains to be determined what is the role played by BRD7 in assembling the PBAF complex and how this complex is assembled to accomplish its function within the immune cells.

In order to investigate the function of BRD7 and its PBAF complex in antiviral immune response, we utilized mice with T cell-specific genetic deficiencies of BRD7 and infected these mice and their littermate wild-type controls with influenza viruses or lymphocytic choriomeningitis virus (LCMV) Armstrong (Arm) viruses, and examined the influence of BRD7 upon T-cell function. We found that the expression of BRD7 was significantly induced in effector $CD8^+$ T cells. BRD7 was not required for the early activation and expansion of $CD8^+$ T cells but was critical for effector differentiation of $CD8^+$ T cells and pathogens clearance during acute viral infection. BRD7-deficient $CD8^+$ T cells failed to initiate the effector T cell transcriptional program and showed impaired cytotoxicity and cytokine production. We therefore demonstrated that BRD7 controls the differentiation of cytotoxic effector $CD8^+$ T cells. Importantly, we identified that BRD7 played a key role in assembling the PBAF complex to perform their functions in effector

$CD8^+$ T cells.

RESULTS

Increased expression of BRD7 in the effector $CD8^+$ T cells

The SWI/SNF complexes are involved in genome-wide transcriptional regulation (16, 17). However, their roles in antiviral immune response remain unknown. To elucidate the roles of SWI/SNF chromatin remodeling complexes in regulating $CD8^+$ T cell responses, we analyzed the expression of components of BAF, PBAF, and ncBAF complexes after influenza virus infection. Among them, we found that the expression of BRD7 was the highest in effector $CD8^+$ T cells at day 10 post infection (p.i.) and the expression maintained high in memory $CD8^+$ T cells (at ~42 days p.i.) from OT-I TCR-transgenic mice when compared to their mRNA expression in naive $CD8^+$ T cells (Fig. 1A). In addition, when we analyzed the kinetics of mRNA expression of several PBAF components during *in vivo* responses to infection, we found that *Brd7* mRNA expression was upregulated at day 6 p.i., and reached the maximum at day 8 (Fig. 1B), suggesting that the expression of BRD7 is concurrent with the development of effector $CD8^+$ T cells. Of note, the $CD8^+$ T cells of these mice recognize a peptide fragment of chicken ovalbumin (OVAp) bound to $H\text{-}2K^b$ when infected with PR8-OVA virus, a recombinant strain of A/PR/8/34 (H1N1) virus expressing ovalbumin. These data therefore indicated that BRD7 in $CD8^+$ T cells may play a critical role in regulating immune response.

In order to examine the role of BRD7 in $CD8^+$ T cell response, we generated mice that conditionally deleted *Brd7* in T cell-specific conditional BRD7 deleted mice ($Brd7^{\Delta T}$) by crossing mice homozygous for *lox*P-flanked alleles of *Brd7* ($Brd7^{fl/fl}$) to mice expressing a transgenic encoding Cre recombinase from T cell-specific *Cd4* promoter (*Cd4-cre*) (Fig. S1), which resulted in lacked expression of BRD7 in mature $CD8^+$ T cells (Fig. S2A). The thymic T cell development and T cell circulation were not affected in $Brd7^{\Delta T}$ mice since similar percentages and absolute numbers of $CD4^+$ and $CD8^+$ T cells were found in thymus, mediastinal lymph nodes (mLN), and spleen from both BRD7-wild-type mice ($Brd7^{fl/fl}$) and BRD7-deleted littermate pairs ($Brd7^{\Delta T}$) (Fig. S2B). To explore the potential for any off-target impacts on related Brd family proteins, we carried out western blotting to scrutinize their expression. The findings revealed that, with the

exception of *Brd7*, the expression of *Brd2*, *Brd4*, *Brg1*, and *Trim-28* remained unaltered in the BRD7-deficient mice (Fig. S3). Thus, this T cell-specific *Brd7* deleted mice allowed us to specifically analyze the role of BRD7 in $CD8^+$ T cell responses during infection.

BRD7 deficiency impairs the differentiation of effector $CD8^+$ T cells

To examine the response of $CD8^+$ T cell subsets of BRD7-sufficient and BRD7-deficient mice during virus infection, we infected $Brd7^{fl/fl}$ mice and $Brd7^{\Delta T}$ mice with the influenza HKx31 strain and analyzed the $CD8^+$ T cells in the spleen and lungs at the peak of the response (Day 10 p.i.). We analyzed influenza antigen-specific $CD8^+$ T cell responses by staining the H-$2D^b$-NP ($NP_{366-374}$) and H-$2D^b$-PA ($PA_{224-233}$) tetramers. There were no obvious differences in the percentages and numbers of the influenza-specific H-$2D^b$-NP^+CD8^+ and H-$2D^b$-PA^+CD8^+ T cells in the spleen and lungs from $Brd7^{fl/fl}$ mice and $Brd7^{\Delta T}$ mice (Fig. 2A-2C). However, the frequency of antigen-specific $KLRG1^+IL7R^-$ SLECs was significantly lower in BRD7-deficient $CD8^+$ T cells than in BRD7-wild-type $CD8^+$ T cells (Fig. 2D and 2E). This finding was not due to tissue distribution since similar results were found in both spleen (Fig. S4A) and the lung (Fig. 2D and 2E). Antigen-specific BRD7-deficient $CD8^+$ T cells also showed increased expression of CD62L and CD27 (Fig. S4B), a defect SLEC differentiation phenotype(7, 39). This phenotype was not due to abnormal activation of $CD8^+$ T cells since the expression of CD69 and CD44 was not altered in BRD7-deficient $CD8^+$ T cells (Fig. S4B). Likewise, to investigate the role of BRD7 in a secondary effector $CD8^+$ T cell response, we used two-infection model in our study. In the primary infection, mice were infected intranasally with the influenza PR8 virus (A/PR/8/34 (H1N1) virus). In the secondary infection, mice were re-challenged with the HKx31 virus intranasally 6 weeks after the first infection. We found that the frequency of NP^+CD8^+ T cells in the lung and spleen was similar between $Brd7^{fl/fl}$ mice and $Brd7^{\Delta T}$ mice (Fig. 2F), while a reduction of antigen-specific $KLRG1^+IL7R^-$ SLECs was found in the $Brd7^{\Delta T}$ mice after infection with HKx31 viruses of previously PR8-primed mice (Fig. 2G). These results indicated a defect in the primary and secondary effector differentiation of $CD8^+$ T cells without BRD7.

To explore whether the defective differentiation of SLECs in BRD7-deficiency mice

depended on the direct role of BRD7 in $CD8^+$ T cells, we generated chimeras by reconstituting lethally irradiated CD45.1 mice with a various 1:1 mixture of bone marrow cells of *Brd7*$^{fl/fl}$ mice and *Brd7*$^{\Delta T}$ mice, followed by infection with HKx31 at 6 week after reconstitution. The frequency of antigen-specific effector $CD8^+$ T cells was analyzed in the spleen of chimeras. We found that the BRD7-deficient $CD8^+$ T cells produced much lower antigen-specific $KLRG1^+$ effector cells than BRD7-wild-type $CD8^+$ T cells did, even in the presence of wild-type $CD8^+$ T cells (Fig. 2H-I), which suggested that BRD7 influenced the differentiation of SLECs depending on the intrinsic role of BRD7 in $CD8^+$ T cells. Furthermore, to rule out the possibility that the deletion of BRD7 in $CD4^+$ T cells may affect the phenotype, we crossed BRD7-deficient mice with mice of the OT-I TCR-transgenic strain to generate OT-I BRD7-deficient mice. The mixture of OT-I BRD7-deficient naïve $CD8^+$ T cells ($CD45.2^+$) and OT-I BRD7-wild-type naïve $CD8^+$ T cells ($CD45.1^+CD45.2^+$) at a ratio of 1:1 was adoptively transferred into CD45.1 mice, followed by infection with PR8-OVA viruses after 24 hours. We found that OT-I BRD7-deficient $CD8^+$ T cells failed to generate as much SLECs as OT-I BRD7-wild-type $CD8^+$ T cells did (Fig. 2J-M). Altogether, these results showed that BRD7 regulated the differentiation in a $CD8^+$ T cell-intrinsic manner.

BRD7 is required for the effector function of $CD8^+$ T cells

After exposure to antigen, activated $CD8^+$ T cells undergo an effector differentiation process and gain the functional ability to produce cytotoxic and effector cytokines to eliminate intracellular pathogens. To examine whether BRD7 deficiency impacts on the effector functions, we measured cytokine production from $CD8^+$ T cells after NP-peptide stimulation by intracellular staining and flow cytometric analysis. The proportion of BRD7-deficient $CD8^+$ T cells producing interferon γ (IFN-γ) (Fig. 3A) and tumor necrosis factor α (TNF-α) (Fig. 3B) was significantly decreased. Likewise, the production of the cytolytic effector molecule GzmB (Fig. 3C) and perforin (Fig. 3D) was hardly detected in antigen-specific BRD7-deficient $CD8^+$ T cells. Low production of these cytolytic effector cytokines will result in a defect in the ability to kill targets. Indeed, BRD7-deficient $CD8^+$ T cells showed a diminished cytolytic effector function in an *in vivo* cytolysis assay (Fig. 3E-F). Of note, in the *in vivo* cytolysis experiment, we stained

splenocytes stimulated with NP peptide by low-dose CFSE ($CFSE^{lo}$ cells) and splenocytes without NP peptide stimulation by high-dose CFSE ($CFSE^{hi}$ cells). Then, we mixed $CFSE^{lo}$ cells and $CFSE^{hi}$ cells at a ratio of 1:1 and injected the mixture into wild-type mice non-infected with HKx31, wild-type mice infected with HKx31, or BRD7-deficient mice infected with HKx31 separately. Almost complete clearance of NP-pulsed cells was observed in wild-type mice infected with HKx31, whereas the killing of these cells was less effective in BRD7-deficient mice infected with HKx31. Similarly, *Brd7*$^{\Delta T}$ mice showed higher degree of weight loss (Fig. 3G) and more severe pathology in the lung than *Brd7*$^{fl/fl}$ mice did after infection with the aggressive influenza PR8 viruses (Fig. 3H). Taken together, these data suggested that BRD7 was required for the production of functional $CD8^+$ effector T cells and the clearance of viruses.

$CD8^+$ T cells will proliferate and differentiate into effector cells to eradicate pathogen during virus infection. This process should be independent of virus strain. To further demonstrate the role of BRD7 in $CD8^+$ T cells response to other viral infection, we further utilized LCMV infection model in our study, which initiates an acute infection. We infected *Brd7*$^{fl/fl}$ mice or *Brd7*$^{\Delta T}$ mice with the Arm strain of LCMV, and analyzed genotypes of mice at the peak of the response (day 8 post infection). Similar percentages and numbers of the LCMV gp33-H-$2D^b$-specific $CD8^+$ T cells were detected in *Brd7*$^{fl/fl}$ and *Brd7*$^{\Delta T}$ mice (Fig. 4A-B), whereas the proportion of antigen-specific $KLRG1^+IL7R^-$ SLECs was fewer in *Brd7*$^{\Delta T}$ mice when compared with littermate controls (Fig. 4C-D). Also, a defect in the production of effector cytokines was detected in $CD8^+$ T cells from *Brd7*$^{\Delta T}$ mice infected with LCMV (Fig. 4E and F). Moreover, a reduced clearance of LCMV virus was observed in *Brd7*$^{\Delta T}$ mice compared to littermate controls (Fig. 4G). These results indicated that BRD7 mediated the SELC development independently of virus strain or TCR specificity.

BRD7 regulates the expression of genes critical for effector differentiation

Cell proliferation and death control the expansion of $CD8^+$ T cells. To explore the proliferation of $CD8^+$ T cells *in vivo* after infection, we evaluated the 5-bromodeoxyuridine (BrdU) incorporation in antigen-specific cells at day 10 after HKx31 infection. We found that the BrdU incorporation of NP^+CD8^+ T cells was similar in

BRD7-deficient and BRD7-wild-type mice (Fig. S5A), indicating that BRD7-deficiency did not alter the proliferation of antigen-specific $CD8^+$ T cells. In addition, when we quantify the apoptotic $CD8^+$ T cells from infected mice using Annexin V and PI staining, we did not find notable differences of the apoptotic antigen-specific $CD8^+$ T cells between BRD7-deficient and wild type mice (Fig. S5B). These data suggested that BRD7 did not mediate cell proliferation or apoptosis of $CD8^+$ T cells, which is consistent with the above data that BRD7 deficiency did not change the proportion of antigen-specific $CD8^+$ T cells.

To better elucidate the underlying molecular mechanism by which BRD7 controls the differentiation of SLECs, we analyzed the global gene expression profiles of BRD7-wild-type and BRD7-deficient antigen-specific $CD8^+$ T cells using RNA sequencing (RNA-seq). We sorted NP^+CD8^+ T cells from *Brd7*$^{fl/fl}$ mice and *Brd7*$^{\Delta T}$ mice infected with HKx31 by flow cytometry at day 10 post infection. BRD7 deficiency led to up-regulation of 856 genes and down-regulation of 647 genes compared to their wild-type counterparts (Fig. 5A). The differential expressed genes were highly enriched among transcripts induced in effector $CD8^+$ T cells and activated $CD8^+$ T cells (Fig. 5B). We also observed a notable different expression in SLEC signature genes, including *Zeb2*, *Tbx21*, *Sell* (*Cd62l*), and *Klrg1* (Fig. 5C). These genes were further categorized as transcription factors, chemokine receptors, adhesion molecules, and killer cell lectin-like receptors (Fig. 5C), indicating that BRD7 exerted broad regulatory effects upon SLEC signature genes.

As an essential component of PBAF complex, BRD7 deficiency may result in the change of chromatin structure. To test this possibility with a higher resolution method, we performed assay of transposase assessable chromatin-sequencing (ATAC-seq), which detects the insert of Tn5 transposase in open chromatin regions(40). ATAC-seq analysis of NP^+CD8^+ T cells showed a less accessible chromatin configuration at SLEC signature genes, including *Zeb2*, *Gzmzb*, and *Ifng* in cells from *Brd7*$^{\Delta T}$ mice than that from *Brd7*$^{fl/fl}$ mice (Fig. 5D), which was consistent with RNA-seq data. The different expression of some important molecules involved in the differentiation of SLECs was further validated by quantitative reverse transcription PCR (qRT-PCR) (Fig. 5E). Consistent with RNA-seq and ATAC-seq data, all these genes were decreased in BRD7-deficient cells compared to

their wild-type counterparts in the effector $CD8^+$ T cells, but not in naïve $CD8^+$ T cells. Altogether, these results revealed that BRD7 was a major regulator of genes involved in SLEC differentiation and function.

PBAF complex enriches at *Tbx21* promoter and impacts T-bet expression in effector $CD8^+$ T cells

Based on the fact that BRD7 is the specific component of PBAF complex, a chromatin remodeling complex, we further examined the chromatin state of the BRD7-bound regions by ChIP-seq with antibodies to BRD7 in BRD7-wild-type OTI $CD8^+$ T cells from OT-I mice infected with PR8-OVA at day 8 p.i.. Notably, we found that BRD7 was enriched at the *Tbx21* loci (Fig. 6A), which was further validated with ChIP-PCR (Fig. 6B). T-bet is a major driver for $CD8^+$ T cell SLEC lineage commitment and controls the expression of a large number of molecules critical for the effector differentiation of $CD8^+$ T cells including *Zeb2*, *Runx3*, *Ifng*, *Gzma* and *Prf1*(5, 41-44). The loss of T-bet leads to abrogated cytotoxic function and influences nearly 50% of the SLEC-specific genes. We hypothesized that BRD7 bound to the *Tbx21* loci and regulated T-bet expression. Indeed, RNA-seq and ATAC-seq revealed a defect in transcriptional activity of *Tbx21* gene after BRD7 deficiency (Fig. 5 and Fig. 6A). A significant decrease of T-bet expression in BRD7-deficient NP^+CD8^+ T cells was also observed by qRT-PCR (Fig. 6C) and flow cytometry analysis (Fig. 6D). Taken together, our results suggested that T-bet acts as the downstream factor for BRD7 to drive during the differentiation of effector cells.

BRD7 was previously reported to bind to H3K9ac (26). To test the possibility that BRD7 binds to H3K9ac and increases the H3K9ac deposition at *Tbx21* locus, we performed ChIP-seq with antibodies to H3K9ac in BRD7-wild-type or BRD7-deficient OTI $CD8^+$ T cells from OT-I mice infected with PR8-OVA at day 8 p.i.. No significant difference of H3K9ac enrichment was observed at *Tbx21* loci in BRD7-deficient cells comparing to BRD7-wild-type cells (Fig. 6A, lowest panel), implying that BRD7 regulated the T-bet expression independent of its binding to H3K9ac. To examine the possibility that the PBAF complex co-opts epigenetic mechanisms for target gene regulation, we further performed ChIP assay with antibodies to H3K9me3, H3K27me3 and H3K14ac on wild-type and BRD7-deficient OTI $CD8^+$ T cells from OT-I mice

infected with PR8-OVA at day 8 p.i.. The H3K9me3, H3K27me3 and H3K14ac modifications at the *Tbx21* locus were not obviously altered after BRD7 deficiency (Fig. 6E). Thus, BRD7 regulated the T-bet expression independent of H3K9me3, H3K27me3 and H3K14ac modification at the *Tbx21* locus.

BRD7 functions as a bridge for PBAF complex to efficiently assembly in effector CD8$^+$ T cells

Based on the result that BRD7 regulated the chromatin accessibility of *Tbx21* locus, we assumed that BRD7 within the PBAF complex plays an important role in effector CD8$^+$ T cell differentiation. To better explore the role of BAF and PBAF complex in CD8$^+$ T cells differentiation, we performed immunoprecipitation with BRG1-specific antibody with lysates from naïve or OTI CD8$^+$ T cells which were from OT-I mice infected with PR8-OVA at day 8 p.i. and were denoted as effector cells. The pull-down substrates were subsequently analyzed with mass spectrometry (Fig. 7A). Being the ATPase subunit of BAF and PBAF complexes, BRG1 is shared by both BAF and PBAF complexes. Therefore, we could observe the component changes of both BAF and PBAF complexes. Interestingly, we found that BAF/PBAF-shared components appeared in the BRG1-associated proteins from both naïve and effector CD8$^+$ T cells (Fig. 7B-7E), while PBAF-specific components including BRD7, PBRM1, PHF10, and ARID2 existed only in that from effector cells (Fig. 7D-E). We further confirmed this result with IP experiment and found that BRG1 interacted with BRD7 only in effector CD8$^+$ T cells, but not in naïve CD8$^+$ T cells (Fig. 7F). Thus, we proposed that the SWI/SNF complexes barely appear as BAF complex in naïve CD8$^+$ T cells and only PBAF complex is assembled in the effector CD8$^+$ T cells.

Because of the chromatin remodeling function, it is reasonable to assume that the ATPase unit of PBAF complex would also be enriched at the loci of target genes. To testify this hypothesis, we used BRG1-specific antibody in the ChIP assay and found that BRG1 specifically enriched at the loci of *Tbx21* in the OTI CD8$^+$ T cells from OT-I mice infected with PR8-OVA at day 8 p.i. (Fig. 7G). Based on the fact that BRG1-deficiency resulted in the loss of double-negative T cells in the thymus during T cell maturation(21), we utilized BRG1-specific shRNA (shBRG1) to specifically deplete BRG1 in mature T

cells. Accordingly, the depletion of BRG1 resulted in a down-regulation of *Tbx21* mRNA expression, indicating that BRG1 plays a role in regulating T-bet. (Fig. 7H and 7I). Thus, we suggested that PBAF complex bound to *Tbx21* loci and regulated the expression of T-bet in the effector $CD8^+$ T cells.

To explore the role of BRD7 within PBAF complex in the effector $CD8^+$ T cells, we further analyzed the interactions between SMARCC1, BRG1, and PBRM1 based on the assembly process of PBAF complex in human 293T cells (17). According to this modular assembly model of PBAF complex, the form of BAF core module and ATPase module are two parallel steps. ATPase module is recruited after the core module incorporation with PBAF specific components ARID2, BRD7, and PHF10. After incorporation with the ATPase module, the PBAF complex intermediate finalizes its formation by binding with PBRM1 (17). However, this model did not propose any role played by BRD7 in assembling PBAF complex. As BRD7 can individually interact with SMARCC1, PBRM1, or BRG1 (17), we supposed that BRD7 may function as a bridge between PBAF core module and ATPase module. To test this hypothesis, we analyzed the interaction between SMARCC1, PBRM1, or BRG1 after BRD7 deficiency in the effector $CD8^+$ T cells. We found that the binding of BRG1 to either SMARCC1 or to PBRM1 became weakened after BRD7 deficiency in the OTI $CD8^+$ T cells (Fig. 7J), indicating that the binding of the core module of BAF- or PBAF-specific component PBRM1 to the ATPase module depended upon BRD7. In addition, the enrichment of BRG1 at *Tbx21* locus was significantly less after BRD7 deficiency in effector $CD8^+$ T cells (Fig. 7K), while the enrichment of SMARCC1 at *Tbx21* locus was unaffected after BRD7 deficiency in effector $CD8^+$ T cells (Fig. 7L), implying that the recruitment of ATPase module to target gene depended on the assembly of the core module of PBAF with BRD7. Altogether, these results indicated that BRD7 was the bridge between BAF core module and ATPase module during the assembly of PBAF complex in effector $CD8^+$ T cells.

DISCUSSION

After antigen stimulation, naïve $CD8^+$ T cells expand and differentiate into effector cytotoxic T cells. Multiple lines of evidence have indicated that T-bet serves as the ‘‘master regulator’’ of SLEC lineage commitment (5, 41-43). T-bet is highly expressed in

effector $CD8^+$ T cells, but lowly expressed in memory $CD8^+$ T cells. It is also required for the production of IFN-γ and the cytotoxicity of $CD8^+$ T cells during LCMV infection. *Tbx21* knockout seriously influences the formation of $KLRG1^{hi}$ subset of effector $CD8^+$ T cells but has little effect on the $IL7R^{hi}$ subset (5, 42). T-bet performs these functions via influencing the expression of many lineage-specific genes expression in SLECs. In the current study, we have identified a prominent role of BRD7 in regulating robust development of effector $CD8^+$ T cells during acute virus infection and functions a key determinant of the switch from naïve T cells to effector T cells. BRD7-deficient $CD8^+$ T cells show impaired expression of effector molecules such as IFN-γ and granzyme B. By RNA-sequencing, ATAC-sequencing, qRT-PCR, and flow cytometry assays, we found that BRD7 sustains the effector differentiation of $CD8^+$ T cells directly through regulating the expression of *Tbx21*. We further demonstrated that BRD7 enriched at the *Tbx21* locus with ChIP assay. These findings indicate that BRD7 affects the development of effector $CD8^+$ T cells through regulating *Tbx21* transcription.

BRD7 has been identified as a tumor-suppressor gene in multiple cancers (28-30, 45-47). High expression Brd7 is associated with improved survivals in multiple cancers. It could recognize and bind to acetylated histone H3 (26). However, several studies also showed that though binding to acetylated histone H3, BRD7 did not have histone acetyltransferases activity (26, 27). In this study, we found that BRD7 regulated the T-bet expression independent of H3K9ac and H3K14ac modifications. We also found that BRD7 regulated the T-bet expression independent of H3K9me3 and H3K27me3 modification at the *Tbx21* locus. However, as BRD7-deficiency decreases the chromatin accessibility of *Tbx21* locus, BRD7 could regulates T-bet expression through altering chromatin modification of *Tbx21* loci as a component of PBAF complex.

Despite many shared components, BAF and PBAF complexes are functionally distinct complexes (23). The balance between BAF and PBAF complexes was reported as a pivotal determinant of the VDR-driven anti-inflammatory response (37). Recently, the researchers found that the BAF complex and c-Myc physically interact to establish the chromatin landscape in activated $CD8^+$ T cells and BAF as a negative determinant of T_{MEM} cell fate (48). In our study, we describe a phenomenon that PBAF- rather than BAF-specific components only exist in effector $CD8^+$ T cells, while did not appear in

naïve $CD8^+$ T cells. The assembly of PBAF complexes was initiated in the effector stage during $CD8^+$ T cells differentiation, which was consistent with the significant upregulation of BRD7 expression in effector $CD8^+$ T cells when compared to naïve $CD8^+$ T cells. PBAF complex functions as chromatin remodelers including nucleosome assembly and organization, chromatin assess and nucleosome editing, which result in their specific interaction with particular transcription activators, repressors and histone modifications. All these factors function together and lead to the activation of a special gene (16, 49). In the presence of BRD7, the proper assembled PBAF complex therefore enhanced the chromatin accessibility at *Tbx21* locus.

A major barrier to our understanding of the functions and tissue-specific roles of mSWI/SNF complex is the lack of knowledge of the assembly and organization of the complex. A significant progress has been made by a recent study (17). This report has posed the modular organization and assembly order of mSWI/SNF complex in human HEK293T cell line. In particular, the assembly of PBAF complex begins with the formation of the core module including SMARCC1, and then incorporates PBAF-specific components ARID2, BRD7, and PHF10 in order. The assembly pathway of PBAF finalizes by recruitment of ATPase module (including BRG1) and the binding of PBRM1. However, the role of BRD7 for the assembly of PBAF in this model remains to be determined. Here we have found that BRD7 interacts with BRG1, SMARCC1, and PBRM1, and is important for BRG1 (ATPase module) and SMARCC1 (core module) interaction. Although BRD7 does not affect the loading of the core module components such as SMARCC1 onto *Tbx21* locus, BRG1 (ATPase module) binds to the *Tbx21* locus in effector $CD8^+$ T cells in a BRD7-dependent manner. These results further confirmed the critical role played by BRD7 in assembling PBAF complex in effector $CD8^+$ T cells, especially at the *Tbx21* locus.

In summary, we found that the major complex of SWI/SNF chromatin-remodeling in effector $CD8^+$ T cells is PBAF complex. Despite many functions of PBAF complex has been illuminated (23), the capability of PBAF complex to mediate SLEC differentiation is unknown. Our study showed the essential role of PBAF complex in SLEC differentiation, and illuminated mechanisms how SLECs maintains the expression of "effector" genes in the presence of PBAF complex. The significantly upregulated BRD7

is the key factor for PBAF assembly in SLECs. However, the signaling pathways that initiate the expression of BRD7 and the mechanism of the switch between BAF and PBAF complexes remain to be illuminated. Nevertheless, our data highlighted the roles of BRD7 and its PBAF complex in the differentiation and function of $CD8^+$ effector cells. By focusing on the BRD7-mediated assembly of PBAF complex in $CD8^+$ T cells, we uncovered a possible therapeutic target to interfering with the induction of functional effector $CD8^+$ T cells, which could open a new avenue for the treatment of various diseases including viral infections, tumors, or autoimmune diseases.

METHODS

Sex as a biological variant

Sex was not considered as a biological variable, both female and male mice were used.

Mice

All mice were on a C57BL/6 (B6) background. *Brd7*$^{fl/fl}$ mice crossed with *Cd4-Cre* mice (*Brd7*$^{\Delta T}$) were used. They were obtained from Shanghai Model Organisms Co. Ltd (Shanghai, China). Cre-negative littermates were used as wild-type controls in all experiments. Wild-type B6 mice, CD45.1 mice and OT-I TCR-transgenic mice were obtained from The Jackson Laboratory. OT-I TCR-transgenic mice, which use a Va_2Vb_5 TCR heterodimer to recognize OVAp (amino acids 257-264) presented by H-2K^b, were congenic for CD45.1 on the B6 background. OT-I CD45.1 mice and *Brd7*$^{\Delta T}$ mice were bred and the offspring were intercrossed to obtain OT-I BRD7-conditional knockout TCR-transgenic mice. During infection experiments, wild-type and BRD7-deficient mice were housed together to avoid 'cage bias'. No intentional method for randomization was used. Chimeras were generated by intravenous injection of 5×10^6 to 10×10^6 donor bone marrow cells (*Brd7*$^{fl/fl}$ and *Brd7*$^{\Delta T}$ cells at a ratio of 1:1) into lethally irradiated CD45.1 mice. *Brd7*$^{fl/fl}$ and *Brd7*$^{\Delta T}$ cells of donor origin were identified with the congenic markers CD45.1 and CD45.2. The chimeras were used at 6 weeks after engraftment. All mice were used at the age of 6-10 weeks, and housed and maintained according to Sun Yat-sen University guidelines (permit number SYXK (YUE) 2010-0107).

Infection with influenza A virus and LCMV-armstrong

For influenza A virus infection, mice were infected intranasally with 10^7 plaque-forming units (PFU) of influenza virus strain A/PR/8/34 (H1N1), the H3N2 influenza A virus strain HKx31, or influenza virus strain A/PR/8/34–OVA (PR8-OVA). To measure recall responses, mice were first inoculated intraperitoneally (i.p.) with 10^7 PFU of the A/PR/8/34 influenza virus and then challenged intranasally (i.n.) with $10^{4.5}$ PFU of HKx31 at 4 weeks later. Virus stocks were grown in the allantoic cavity of 10 days embryonated hen's eggs and stored in aliquots at -80°C. Viral titers were obtained by

infection of MDCK (Mardin-Darby canine kidney) cells as previously described(50, 51). MDCK cells were obtained from American Type Culture Collection (ATCC).

For LCMV-Armstrong infection, mice were generally infected intraperitoneally with LCMV Arm strain (1×10^6 to 5×10^6 PFU). Eight days after infection, mice were euthanized and donor cells were assessed using LCMV-$GP^{33–41}$-tetramer (H-$2D^b$-$GP33^+$) staining.

Flow cytometry and cell sorting

Single-cell suspensions were prepared from spleen, or lung. The following antibodies were used (All monoclonal antibodies from eBioscience): anti-CD3ε (145-2C11), anti-CD4 (GK1.5), anti-CD8a (53-6.7), anti-KLRG1 (2F1), anti-CD127 (anti-IL7Rα; A7R34), anti-CD45.1(A20), anti-CD45.2 (104), anti-CD62L (MEL-14), anti-CD44 (IM7), anti-CD69 (H1.2F3), anti-CD27 (LG.7F9), anti-BrdU (BU20A), anti-IFN-γ (XMG1.2), anti-TNF-α (MP6-XT22), anti-granzyme B (NGZB), anti-Perforin (dG9 (delta G9)), and anti-T-bet (4B10). Allophycocyanin-conjugated tetramers of H-$2D^b$ used in the study were all from Helixgen (Guangzhou) Co., Ltd: anti-Flu.NP_{366} (ASNENMETM), anti-Flu. PA_{224} (SSLENFRAYV), and anti-LCMV-GP_{33} (KAVYNFATM).

For measurement of intracellular cytokine expression, splenocytes were isolated *ex vivo* and stimulated with 1 µg/ml of the major histocompatibility complex class I (MHC- I)–restricted influenza-derived peptide NP (amino acids 366–374 (ASNENMETM)) in IMDM media plus 10% FBS with 50 ng/ml PMA (Sigma-Aldrich), 1 µg/ml ionomycin (Sigma-Aldrich), and 1 µg/ml brefeldin A (eBioscience) for 4-6 h. Cells were stained for 20 min at room temperature with the relevant fluorochrome-conjugated monoclonal antibodies in PBS containing 0.5% BSA. For intracellular staining, cells were fixed and permeabilized with Cytofix/Cytoperm (BD Biosciences), and stained with antibodies against indicated cytokines. For staining of transcription factor, cells were stained with antibodies to surface antigens, fixed and permeabilized according to the manufacturer's instructions (Transcription Factor Staining Buffer Set; BD Biosciences). Cells were acquired on an LSRFortessa flow cytometer (BD Bioscience), and data were analyzed with the FlowJo V10.0.7 (FlowJo). The fraction of labeled cells was analyzed with a minimum 100,000 events.

For the flow cytometric sorting, a BD FACSAriaIII cell sorter (BD Bioscience) was used. For the isolation of H-2D^{b}-NP tetramer-positive CD8^{+} T cells from influenza virus infected mice, single-cell suspensions of lung were stained with influenza virus–specific tetramers and antibodies to the relevant markers. For the isolation of naïve CD8^{+} T cells from B6 mice, single-cell susupensions of spleen with stained with the specific fluorochrome-conjugated antibodies. All the cells were sorted with a purity ≥95%.

Adoptive transfer of CD8^{+} T cells and Infections

Congenically distinct *Brd7*$^{fl/fl}$ and *Brd7*$^{\Delta T}$ OT-I CD8^{+} T cells were mixed at a 1:1 ratio and adoptively transferred at 1 × 10^{5} cells per CD45.1 recipient mouse. Mice were then infected intranasally with PR8–OVA virus.

Generation of Bone Marrow chimeras

For *Brd7*$^{fl/fl}$: *Brd7*$^{fl/fl}$ or *Brd7*$^{fl/fl}$: *Brd7*$^{\Delta T}$ chimeras, CD45.1^{+} mice were lethally irradiated with 950 rad and then injected intravenously (i.v.) with 1 × 10^{7} bone marrow cells harvested from *Brd7*$^{fl/fl}$ CD45.2^{+} and *Brd7*$^{fl/fl}$ CD45.1^{+}CD45.2^{+} or *Brd7*$^{\Delta T}$ CD45.2^{+} and *Brd7* $^{fl/fl}$ CD45.1^{+}CD45.2^{+} littermates at the ratio of 1:1. The mice were treated with sulfamethoxazole and trimethoprim (Bactrim) antibiotics diluted in drinking water for 4 weeks after reconstitution. After approximately 6 weeks, the mice were infected with HKx31 virus, and sacrificed for flow cytometry analysis at 10 p.i..

***In vivo* cytotoxicity assay**

Target spleen cells from B6 mice were pulsed for 30 min with 1 µg/ml influenza virus-derived NP peptide (amino acids 366–374) and were subsequently labeled for 20 min at 37 °C with 0.2 µM CFSE (carboxyfluorescein diacetate succinimidyl ester; Invitrogen) (CFSE^{lo}; specific target cells) or were not pulsed with peptide and were labeled with 2 µM CFSE (CFSE^{hi}; nonspecific target cells). The two target populations were mixed in equal numbers, and 5×10^{6} cells were transferred i.n. into mice that had been infected with influenza A virus HKx31 strain 10 d before or into non-infected control mice. Mice were killed 4 h later and the ratio of peptide-loaded target cells to ‘empty’ target cells was quantified by flow cytometry.

RNA-Seq and ATAC-Seq

$CD8^+$ T cells that bound H-$2D^b$-NP (NP peptide amino acids 366-374) were isolated by flow cytometry from lung of influenza virus-infected wild type or BRD7-deficient mice. Total RNAs from each group were extracted by TRIzol Reagent (ThermoFisher) according to the manufacturer's instruction. The quality of RNA samples were evaluated by Nanodrop 2000 (ThermoFisher) and BioAnalyzer 2100 (Aglient). The RNA-Seq library were built with TruSeq Stranded mRNA Library Prep Kit (Illumina) and sequenced with HiSeq X Ten (Illumina) at BioMarker (Beijing, China) under the PE150 protocol(52). RNA-Seq reads were trimmed, filtered and quality-controlled by FastQC (Babraham Institute) tool. The reads were aligned to mouse reference genome NCBI build 38 (GRCm38) by Hisat2, followed by calculating the reads per kilobase per million mapped reads (RPKM).

ATAC-Seq was conducted with H-$2D^b$-NP^+CD8^+ T cells of influenza virus-infected wild type and BRD7-deficient mice. The ATAC-Seq library was built with TruePrep DNA Library Prep Kit V2 (Vazyme) as previously described(52). In brief, the library quality was evaluated by Qubit 3.0 Fluorometer (ThermoFisher) and BioAnalyzer 2100 (Aglient), and sequenced with HiSeq X Ten (Illumina) at BioMarker (Beijing, China) under the PE150 protocol. ATAC-Seq reads were trimmed, filtered and quality-controlled by FastQC tool. Then the reads were aligned to GRCm38 by Bowtie2 (Langmead and Salzberg, 2012), followed by rearranging with Samtools. Igvtools (Broad Institute) was used to visualize the tag peaks. Specific gene loci were amplified. Tag density from different groups was calculated by normalizing to the total mapped reads.

ChIP-seq and ChIP-qPCR

ChIP was performed according to the manufacturer's instruction (Cell Signaling Technology). In brief, naive OT-I $CD8^+$ T cells or OT-I $CD8^+$ cells from OT-I mice infected with PR8-OVA at day 8 p.i. fixed with 1% formaldehyde (Sigma-Aldrich), followed by digestion with RNase cocktail. Chromatin from 5×10^6 to 10×10^6 cells was used for each ChIP experiment. Antibodies against normal rabbit IgG (1:50, Cat No. 2729, Cell Signaling Technology), BRD7 mouse mAb (1:50, (B-8), Cat No. sc-376180, Santa

Cruz), BRG1 Rabbit mAb (1:50, (D1Q7F), Cat No. 49360, Cell Signaling Technology), H3K9ac Rabbit mAb (1:50, (C5B11), Cat No. 9649, Cell Signaling Technology), H3K14ac Rabbit mAb (1:50, (D4B9), Cat No. 7627, Cell Signaling Technology), H3K9me3 Rabbit mAb (1:50, (D4W1U), Cat No. 13969, Cell Signaling Technology) and H3K27me3 Rabbit mAb (1:50, (C36B11), Cat No. 9733, Cell Signaling Technology) were used. Antibody-DNA complexes were captured by ChIP-Grade Protein G Magnetic Beads. The immunoprecipitated DNA was purified and subjected to sequencing or PCR assessment. ChIP primers targeting the *Tbx21* were used to quantitate each target regions by Quantitative RT-PCR.

Quantitative RT-PCR

Total RNA from indicated numbers of cells were isolated with TRIzol reagent (Thermo Fisher) and preceded to cDNA synthesis with PrimeScript RT reagent Kit (Takara). Gene expression was analyzed by Real-time PCR with SYBR Ex-taq premix (Takara) in a CFX96 Real-time PCR Detection System (Bio-Rad). Mouse β-actin mRNA was measured as internal control.

Mass spectrometry

Mass spectrometry analysis was performed as previously described(50). In brief, the stained bands of interest were excised into gel slices with a clean scalpel, followed by digested with trypsin using in-gel digestion. Each gel piece was diced into small (1-mm3) pieces, and dehydrated. The gel pieces were then incubated with trypsin (Promega) for digestion. Peptides were further extracted with 50% acetonitrile-5% formic acid, lyophilized in a SpeedVac (Thermo Savant), and then desalted using u-C18 Ziptip (Millipore). Finally, samples were lyophilized and stored at 20°C prior to analysis by LC-MS/MS or dissolved in 0.1% (vol/vol) formic acid-water. All samples were analyzed on a Thermo Scientific Q EXACTIVE massspectrometer coupled with an EASY n-LC 1000 liquid chromatography (ThermoFisher) system and a nanoelectrospray source.

Coimmunoprecipitation (co-IP) and western blot assays.

Co-IP and western blot assays were performed as previously described (50). Wild-type

(*Brd7*$^{fl/fl}$) or BRD7-deficient OT-I CD8$^+$ T cells from OT-I mice infected with PR8-OVA at day 8 p.i. were collected and lysed. The lysates were precleared with protein A/G agarose beads (Millipore) for 30 min and then incubated with anti-BRG1 antibody or rabbit normal IgG antibody for 6 h to overnight, followed by incubating with protein A/G agarose beads (Millipore) for 4 h at 4°C. The beads were then washed three times with ice-cold lysis buffer, followed by Western blotting. The following antibodies were used: β-actin antibody (1:1000, Cat No. 4967, Cell Signaling Technology), BRD7 mouse mAb (1:500, (B-8), Cat No. sc-376180, Santa Cruz), BRG1 Rabbit mAb (1:500, (D1Q7F), Cat No. 49360, Cell Signaling Technology), BRD2 Rabbit mAb (1:500, (D89B4), Cat No. 5848, Cell Signaling Technology), BRD4 Rabbit mAb (1:500, (E2A7X), Cat No. 13440, Cell Signaling Technology), TRIM28 Polyclonal antibody (1:500, Cat No. 15202-1-AP, Proteintech), IRDye 680RD Goat anti-Mouse IgG (H + L), 0.5 mg Antibody (1:10000, Cat No. 926–68070, LI-COR Biosciences), IRDye 800CW Goat Anti-Rabbit IgG, Conjugated Antibody(1:10000, Cat No. 926–32211, LI-COR Biosciences).

shRNA-mediated knockdown by retroviral transduction

DNA fragments encoding shRNA targeting mouse BRG1 (SMARCA4) were subcloned into a custom retroviral vector containing GFP as a reporter (pMKO.1). CD8$^+$ T cells of OT-I mice were separated and stimulated for 18 h in 24-well plates precoated with anti-CD3 and anti-CD28. After stimulation, cells were transduced by adding retroviral supernatants supplemented with 100 U/ml mouse IL-2 and 8 μg/ml polybrene, followed by centrifugation for 95 min at 950 g at 32°C. After transduction, cells were incubated for 12-16 h at 37°C. 1 × 10^5 transduced CD8$^+$ T cells were transferred into PR8-OVA virus infected hosts (CD45.1 mice) at day 1 p.i., and remaining cells were cultured in vitro with 50 U/ml human IL-2 for 2 d to assess for knockdown efficiency by qPCR. At 10 d after infection, CD45.2$^+$ populations were assessed by flow cytometry.

Statistical analysis

All data are derived from two to three independent experiments. Statistical analysis was performed with GraphPad Prism 5.0 software (GraphPad Software, La Jolla, CA). Results show mean ± s.e.m. Two-tailed student’s t-test was used to compare two

independent groups, while two-way ANOVA was used in multiple comparisons. Differences were considered significant when *P<0.05, **P<0.01, ***P<0.001 and ****P<0.0001.

Study approval

All mouse experimental procedures were approved by the Institutional Animal Care and Use Committee of Sun Yat-sen University (Guangzhou, China).

Data Availability

All datasets generated or analyzed during this study have included in this manuscript. The RNA-seq , ATAC-seq and ChIP-seq data have been deposited in the Sequence Read Archive (SRA) database (accession number PRJNA1122236 and PRJNA1122318). The data are available in the “Supporting data values” XLS file and from the corresponding author on reasonable request.

CONFLICT OF INTEREST

The authors declare no conflict of interest.

AUTHOR CONTRIBUTIONS

F.H, YT.L, YD. Q and YC.Y designed the experiments, performed most of these experiments, analyzed the data, and manuscript writing; ZH.Z, BH.L, YT. W, J.L, JL.C and WY.Z performed some of the experiments; H.Z provided scientific expertise and the interpretation of data for the work; BF. L contributed to the idea generation, experimental design, manuscript writing and conceived the project.

FUNDINGS

National key research and development program (2021YFC2301904), and Basic and Applied Basic Research Fund Committee of Guangdong Province (SL2022A04J01923) to BF.L; National Key R&D Program of Department of Science and Technology of China (2022YFC0870700), Important Key Program of Natural Science Foundation of China (NSFC) (92169201, 92369205), Emergency Key Program of Guangzhou National

Laboratory (EKPG21-24), and Key R&D Program of Department of Science and Technology of Guangdong (2022B1111020004) to H.Z.

ACKNOWLEDGMENTS

We gratefully acknowledge Dr. Lilin Ye (Institute of Immunology, Third Military Medical University, Chongqing, China) for providing the LCMV Arm virus.

REFERENCES

1. Gray SM, Kaech SM, and Staron MM. The interface between transcriptional and epigenetic control of effector and memory CD8(+) T-cell differentiation. *Immunol Rev.* 2014;261(1):157-68.
2. Kaech SM, and Cui W. Transcriptional control of effector and memory CD8+ T cell differentiation. *Nat Rev Immunol.* 2012;12(11):749-61.
3. Chang JT, Wherry EJ, and Goldrath AW. Molecular regulation of effector and memory T cell differentiation. *Nat Immunol.* 2014;15(12):1104-15.
4. Rutishauser RL, and Kaech SM. Generating diversity: transcriptional regulation of effector and memory CD8 T-cell differentiation. *Immunol Rev.* 2010;235(1):219-33.
5. Joshi NS, Cui W, Chandele A, Lee HK, Urso DR, Hagman J, et al. Inflammation directs memory precursor and short-lived effector CD8(+) T cell fates via the graded expression of T-bet transcription factor. *Immunity.* 2007;27(2):281-95.
6. Cannarile MA, Lind NA, Rivera R, Sheridan AD, Camfield KA, Wu BB, et al. Transcriptional regulator Id2 mediates CD8+ T cell immunity. *Nat Immunol.* 2006;7(12):1317-25.
7. Kallies A, Xin A, Belz GT, and Nutt SL. Blimp-1 transcription factor is required for the differentiation of effector CD8(+) T cells and memory responses. *Immunity.* 2009;31(2):283-95.
8. Yang CY, Best JA, Knell J, Yang E, Sheridan AD, Jesionek AK, et al. The transcriptional regulators Id2 and Id3 control the formation of distinct memory CD8+ T cell subsets. *Nat Immunol.* 2011;12(12):1221-9.
9. Yao S, Buzo BF, Pham D, Jiang L, Taparowsky EJ, Kaplan MH, et al. Interferon regulatory factor 4 sustains CD8(+) T cell expansion and effector differentiation. *Immunity.* 2013;39(5):833-45.
10. Hess Michelini R, Doedens AL, Goldrath AW, and Hedrick SM. Differentiation of CD8 memory T cells depends on Foxo1. *J Exp Med.* 2013;210(6):1189-200.
11. Kim MV, Ouyang W, Liao W, Zhang MQ, and Li MO. The transcription factor Foxo1 controls central-memory CD8+ T cell responses to infection. *Immunity.* 2013;39(2):286-97.
12. Pearce EL, Mullen AC, Martins GA, Krawczyk CM, Hutchins AS, Zediak VP, et al. Control of effector CD8+ T cell function by the transcription factor Eomesodermin. *Science.* 2003;302(5647):1041-3.
13. Zhou X, Yu S, Zhao DM, Harty JT, Badovinac VP, and Xue HH. Differentiation and persistence of memory CD8(+) T cells depend on T cell factor 1. *Immunity.* 2010;33(2):229-40.
14. Gray SM, Amezquita RA, Guan T, Kleinstein SH, and Kaech SM. Polycomb Repressive Complex 2-Mediated Chromatin Repression Guides Effector CD8(+) T Cell Terminal Differentiation and Loss of Multipotency. *Immunity.* 2017;46(4):596-608.
15. Shin HM, Kapoor V, Guan T, Kaech SM, Welsh RM, and Berg LJ. Epigenetic modifications induced by Blimp-1 Regulate CD8(+) T cell memory progression during acute virus infection. *Immunity.* 2013;39(4):661-75.
16. Clapier CR, Iwasa J, Cairns BR, and Peterson CL. Mechanisms of action and regulation of ATP-dependent chromatin-remodelling complexes. *Nat Rev Mol Cell Biol.* 2017;18(7):407-22.
17. Mashtalir N, D'Avino AR, Michel BC, Luo J, Pan J, Otto JE, et al. Modular Organization and Assembly of SWI/SNF Family Chromatin Remodeling Complexes. *Cell.* 2018;175(5):1272-88 e20.
18. Sokpor G, Nguyen HP, and Tuoc T. Context-specific chromatin remodeling activity of mSWI/SNF complexes depends on the epigenetic landscape. *Signal Transduct Target Ther.* 2021;6(1):360.
19. Mashtalir N, Dao HT, Sankar A, Liu H, Corin AJ, Bagert JD, et al. Chromatin landscape signals differentially dictate the activities of mSWI/SNF family complexes. *Science.* 2021;373(6552):306-15.
20. Yuan J, Chen K, Zhang W, and Chen Z. Structure of human chromatin-remodelling PBAF complex bound to a nucleosome. *Nature.* 2022;605(7908):166-71.
21. Gebuhr TC, Kovalev GI, Bultman S, Godfrey V, Su L, and Magnuson T. The role of Brg1, a catalytic subunit of mammalian chromatin-remodeling complexes, in T cell development. *J Exp Med.* 2003;198(12):1937-49.
22. Zhang F, and Boothby M. T helper type 1-specific Brg1 recruitment and remodeling of nucleosomes positioned at the IFN-gamma promoter are Stat4 dependent. *J Exp Med.* 2006;203(6):1493-505.

23. Hodges C, Kirkland JG, and Crabtree GR. The Many Roles of BAF (mSWI/SNF) and PBAF Complexes in Cancer. *Cold Spring Harb Perspect Med.* 2016;6(8).
24. Osman S. Reshuffling chromatin: how the human chromatin remodeler PBAF recognizes nucleosomes. *Nat Struct Mol Biol.* 2022;29(5):419.
25. Kaeser MD, Aslanian A, Dong MQ, Yates JR, 3rd, and Emerson BM. BRD7, a novel PBAF-specific SWI/SNF subunit, is required for target gene activation and repression in embryonic stem cells. *J Biol Chem.* 2008;283(47):32254-63.
26. Sun H, Liu J, Zhang J, Shen W, Huang H, Xu C, et al. Solution structure of BRD7 bromodomain and its interaction with acetylated peptides from histone H3 and H4. *Biochem Biophys Res Commun.* 2007;358(2):435-41.
27. Peng C, Zhou J, Liu HY, Zhou M, Wang LL, Zhang QH, et al. The transcriptional regulation role of BRD7 by binding to acetylated histone through bromodomain. *J Cell Biochem.* 2006;97(4):882-92.
28. Burrows AE, Smogorzewska A, and Elledge SJ. Polybromo-associated BRG1-associated factor components BRD7 and BAF180 are critical regulators of p53 required for induction of replicative senescence. *Proc Natl Acad Sci U S A.* 2010;107(32):14280-5.
29. Chiu YH, Lee JY, and Cantley LC. BRD7, a tumor suppressor, interacts with p85alpha and regulates PI3K activity. *Mol Cell.* 2014;54(1):193-202.
30. Drost J, Mantovani F, Tocco F, Elkon R, Comel A, Holstege H, et al. BRD7 is a candidate tumour suppressor gene required for p53 function. *Nat Cell Biol.* 2010;12(4):380-9.
31. Hu K, Wu W, Li Y, Lin L, Chen D, Yan H, et al. Poly(ADP-ribosyl)ation of BRD7 by PARP1 confers resistance to DNA-damaging chemotherapeutic agents. *EMBO Rep.* 2019;20(5).
32. Wang XM, Wang YC, Liu XJ, Wang Q, Zhang CM, Zhang LP, et al. BRD7 mediates hyperglycaemia-induced myocardial apoptosis via endoplasmic reticulum stress signalling pathway. *J Cell Mol Med.* 2017;21(6):1094-105.
33. Zhao R, Liu Y, Wang H, Yang J, Niu W, Fan S, et al. BRD7 plays an anti-inflammatory role during early acute inflammation by inhibiting activation of the NF-small ka, CyrillicB signaling pathway. *Cell Mol Immunol.* 2017;14(10):830-41.
34. Kikuchi M, Okumura F, Tsukiyama T, Watanabe M, Miyajima N, Tanaka J, et al. TRIM24 mediates ligand-dependent activation of androgen receptor and is repressed by a bromodomain-containing protein, BRD7, in prostate cancer cells. *Biochim Biophys Acta.* 2009;1793(12):1828-36.
35. Chirkova T, Lin S, Oomens AG, Gaston KA, Boyoglu-Barnum S, Meng J, et al. CX3CR1 is an important surface molecule for respiratory syncytial virus infection in human airway epithelial cells. *The Journal of general virology.* 2015;96(9):2543-56.
36. Smith JJ, Xiao Y, Parsan N, Medwig-Kinney TN, Martinez MAQ, Moore FEQ, et al. The SWI/SNF chromatin remodeling assemblies BAF and PBAF differentially regulate cell cycle exit and cellular invasion in vivo. *PLoS Genet.* 2022;18(1):e1009981.
37. Wei Z, Yoshihara E, He N, Hah N, Fan W, Pinto AFM, et al. Vitamin D Switches BAF Complexes to Protect beta Cells. *Cell.* 2018;173(5):1135-49 e15.
38. Pan D, Kobayashi A, Jiang P, Ferrari de Andrade L, Tay RE, Luoma AM, et al. A major chromatin regulator determines resistance of tumor cells to T cell-mediated killing. *Science.* 2018;359(6377):770-5.
39. Hikono H, Kohlmeier JE, Takamura S, Wittmer ST, Roberts AD, and Woodland DL. Activation phenotype, rather than central– or effector–memory phenotype, predicts the recall efficacy of memory CD8⁺ T cells. *The Journal of experimental medicine.* 2007;204(7):1625-36.
40. Buenrostro JD, Giresi PG, Zaba LC, Chang HY, and Greenleaf WJ. Transposition of native chromatin for fast and sensitive epigenomic profiling of open chromatin, DNA-binding proteins and nucleosome position. *Nat Methods.* 2013;10(12):1213-8.
41. Kallies A, and Good-Jacobson KL. Transcription Factor T-bet Orchestrates Lineage Development and Function in the Immune System. *Trends Immunol.* 2017;38(4):287-97.
42. Xin A, Masson F, Liao Y, Preston S, Guan T, Gloury R, et al. A molecular threshold for effector CD8(+) T cell differentiation controlled by transcription factors Blimp-1 and T-bet. *Nat Immunol.* 2016;17(4):422-32.
43. Dominguez CX, Amezquita RA, Guan T, Marshall HD, Joshi NS, Kleinstein SH, et al. The

transcription factors ZEB2 and T-bet cooperate to program cytotoxic T cell terminal differentiation in response to LCMV viral infection. *J Exp Med.* 2015;212(12):2041-56.
44. Omilusik KD, Best JA, Yu B, Goossens S, Weidemann A, Nguyen JV, et al. Transcriptional repressor ZEB2 promotes terminal differentiation of CD8+ effector and memory T cell populations during infection. *J Exp Med.* 2015;212(12):2027-39.
45. Xiao L, Parolia A, Qiao Y, Bawa P, Eyunni S, Mannan R, et al. Targeting SWI/SNF ATPases in enhancer-addicted prostate cancer. *Nature.* 2022;601(7893):434-9.
46. Carcamo S, Nguyen CB, Grossi E, Filipescu D, Alpsoy A, Dhiman A, et al. Altered BAF occupancy and transcription factor dynamics in PBAF-deficient melanoma. *Cell Rep.* 2022;39(1):110637.
47. Shu S, Wu HJ, Ge JY, Zeid R, Harris IS, Jovanović B, et al. Synthetic Lethal and Resistance Interactions with BET Bromodomain Inhibitors in Triple-Negative Breast Cancer. *Mol Cell.* 2020;78(6):1096-113.e8.
48. Guo A, Huang H, Zhu Z, Chen MJ, Shi H, Yuan S, et al. cBAF complex components and MYC cooperate early in CD8(+) T cell fate. *Nature.* 2022;607(7917):135-41.
49. Barisic D, Stadler MB, Iurlaro M, and Schubeler D. Mammalian ISWI and SWI/SNF selectively mediate binding of distinct transcription factors. *Nature.* 2019;569(7754):136-40.
50. Zhang J, Huang F, Tan L, Bai C, Chen B, Liu J, et al. Host Protein Moloney Leukemia Virus 10 (MOV10) Acts as a Restriction Factor of Influenza A Virus by Inhibiting the Nuclear Import of the Viral Nucleoprotein. *Journal of virology.* 2016;90(8):3966-80.
51. Huang F, Chen J, Zhang J, Tan L, Lu G, Luo Y, et al. Identification of a novel compound targeting the nuclear export of influenza A virus nucleoprotein. *J Cell Mol Med.* 2018;22(3):1826-39.
52. Ma X, Yang T, Luo Y, Wu L, Jiang Y, Song Z, et al. TRIM28 promotes HIV-1 latency by SUMOylating CDK9 and inhibiting P-TEFb. *Elife.* 2019;8.

FIGURE LEGENDS

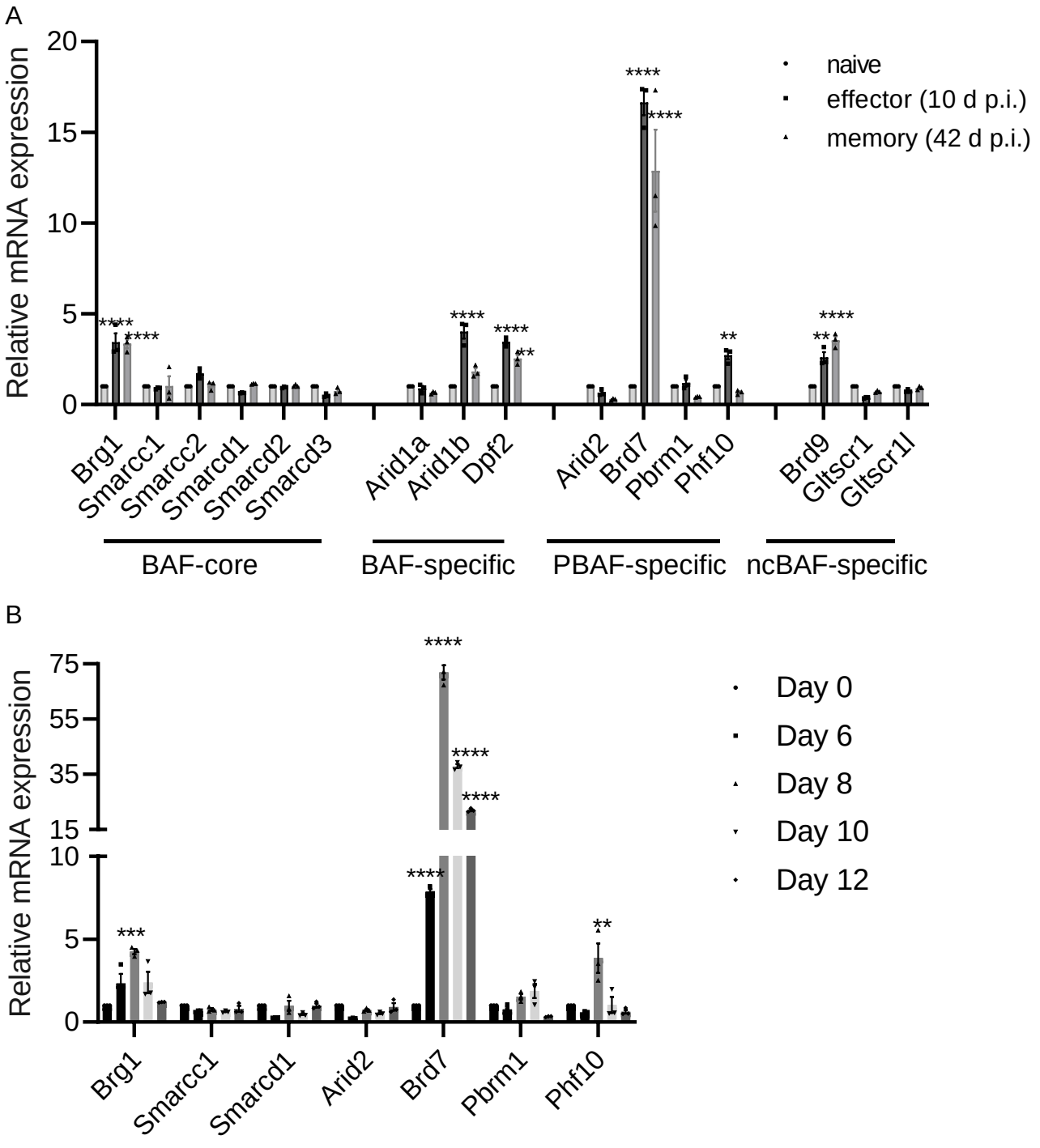
A
Relative mRNA expression
20
15
10
5
0
naive
effector (10 d p.i.)
memory (42 d p.i.)
Brg1
Smarcc1
Smarcc2
Smarcd1
Smarcd2
Smarcd3
Arid1a
Arid1b
Dpf2
Arid2
Brd7
Pbrm1
Phf10
Brd9
Gltscr1
Gltscr1l
BAF-core
BAF-specific
PBAF-specific
ncBAF-specific
B
Relative mRNA expression
75
55
35
15
10
5
0
Day 0
Day 6
Day 8
Day 10
Day 12
Brg1
Smarcc1
Smarcd1
Arid2
Brd7
Pbrm1
Phf10

Figure 1

FIGURE 1. BRD7 is upreguated in effector CD8$^+$ T cells. (**A**) Differential expression of relative mRNAs in naïve, effector and memory OT-I CD8$^+$ T cells was analyzed. Naïve OT-I cells purified from spleen of OT-I mice were transferred into recipient CD45.1 mice and then infected with PR8-OVA at day 1 after transfer. Effector (10 d p.i.) and memory (~42 d p.i.) OT-I cells were purified with FACS for mRNA quantification relative to that of naïve OT-I cells. (**B**) Time course of mRNA expression of several PBAF components in OT-I T cells purified from spleen of OT-I mice which were transferred into recipient CD45.1 mice and then infected with PR8-OVA at day 1 after transfer. *P<0.05, **P<0.01, ***P<0.001 and ****P<0.0001 (Two-way ANOVA). Mean and s.e.m. of three mice per group. Data are representative of two independent experiments.

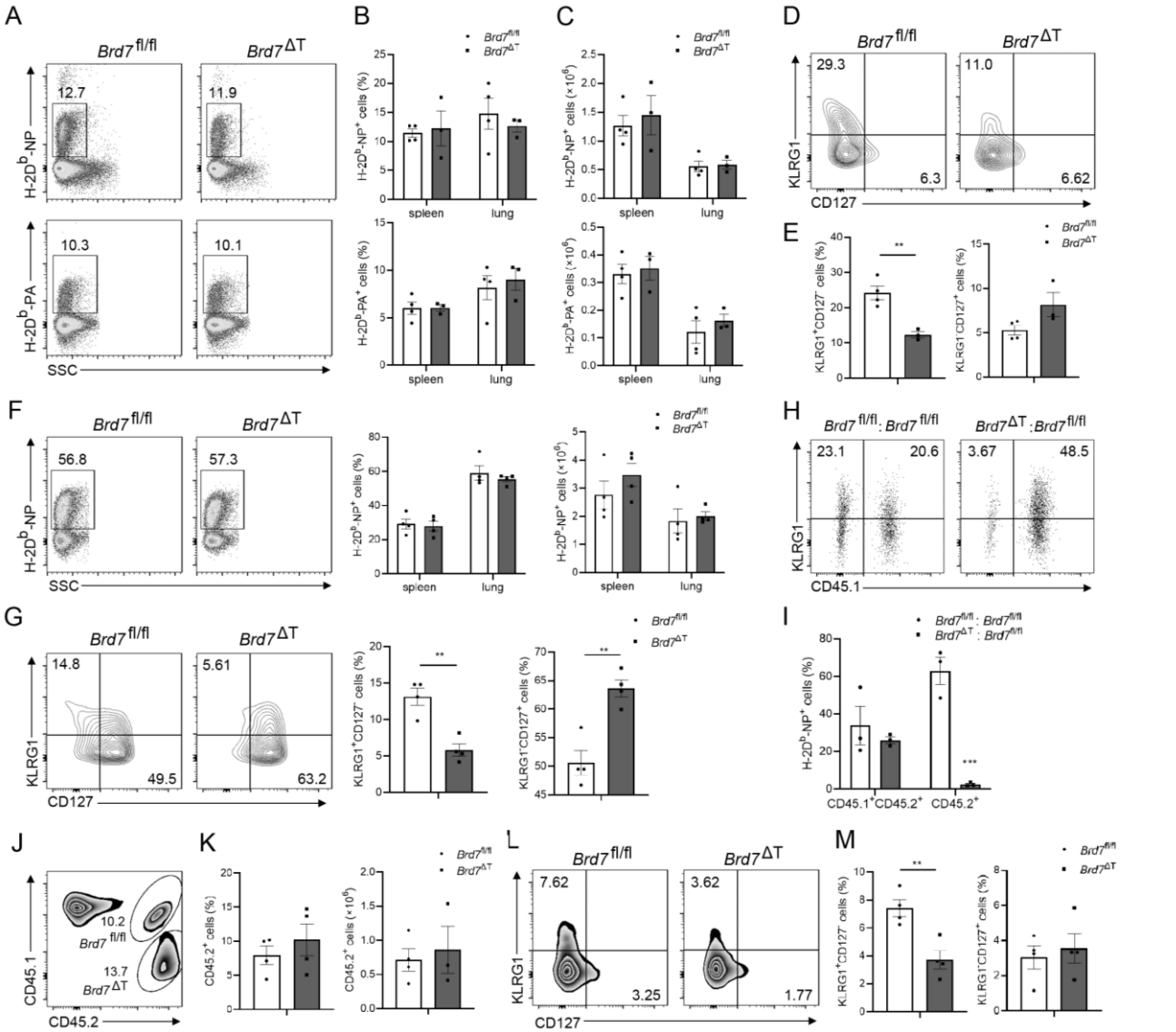
A
Brd7 fl/fl
Brd7 ΔT
12.7
11.9
10.3
10.1
H-2D^b-NP
H-2D^b-PA
SSC
B
Brd7 fl/fl
Brd7 ΔT
H-2D^b-NP+ cells (%)
H-2D^b-PA+ cells (%)
spleen
lung
C
H-2D^b-NP+ cells (×10^6)
H-2D^b-PA+ cells (×10^6)
D
29.3
6.3
11.0
6.62
KLRG1
CD127
E
KLRG1+CD127- cells (%)
KLRG1-CD127+ cells (%)
F
56.8
57.3
G
14.8
49.5
5.61
63.2
KLRG1+CD127- cells (%)
KLRG1-CD127+ cells (%)
H
Brd7 fl/fl : Brd7 fl/fl
Brd7 ΔT : Brd7 fl/fl
23.1
20.6
3.67
48.5
CD45.1
I
Brd7 fl/fl : Brd7 fl/fl
Brd7 ΔT : Brd7 fl/fl
H-2D^b-NP+ cells (%)
CD45.1+CD45.2+
CD45.2+
J
10.2
Brd7 fl/fl
13.7
Brd7 ΔT
CD45.1
CD45.2
K
CD45.2+ cells (%)
CD45.2+ cells (×10^6)
L
7.62
3.25
3.62
1.77
M
KLRG1+CD127- cells (%)
KLRG1-CD127+ cells (%)

Figure 2

FIGURE 2. BRD7 controls SLEC differentiation. (**A**) Flow cytometry of influenza H-2D^{b}-NP^{+}CD8^{+} and H-2D^{b}-PA^{+}CD8^{+} T cells from spleen and lungs of BRD7-wild-type (*Brd7*$^{fl/fl}$) (n=4) and BRD7-deficient (*Brd7*$^{\Delta T}$) (n=3) mice. Mice were infected with influenza HKx31 virus, and NP366 and PA244 tetramer were stained in lung, spleen CD8^{+} T cells at 10 d p.i.. (**B-C**) Frequency and cell number of H-2D^{b}-NP^{+} or H-2D^{b}-PA^{+} cells among CD8^{+} T cells in **A**. (**D-E**) Flow cytometry of KLRG1 and CD127 on H-2D^{b}-NP^{+}CD8^{+} T cells in the lungs obtained from *Brd7*$^{fl/fl}$ (n=4) or *Brd7*$^{\Delta T}$ (n=3) mice infected with HKx31 at 10 d p.i.. (**F**) Flow cytometry of H-2D^{b}-NP^{+}CD8^{+} T cells from spleen and lungs of PR8-primed *Brd7*$^{fl/fl}$ (n=4) and *Brd7*$^{\Delta T}$ (n=4) mice rechallenged with HKx31 at 6 weeks after PR8 infection. (**G**) Flow cytometry of KLRG1 and CD127 on H-2D^{b}-NP^{+}CD8^{+} T cells in the spleen obtained of PR8-primed *Brd7*$^{fl/fl}$ (n=4) and *Brd7*$^{\Delta T}$ (n=4) mice rechallenged with HKx31 at 6 weeks after PR8 infection. (**H-I**) Flow cytometry of KLRG1 and CD45.1 on NP^{+}CD8^{+} T cells from chimeras. Mixed bone marrow chimeras were generated by reconstitution lethally irradiated CD45.1 mice with bone marrow from *Brd7*$^{fl/fl}$ (CD45.2^{+}) plus *Brd7*$^{fl/fl}$ (CD45.1^{+}CD45.2^{+}) (n=3), or *Brd7*$^{\Delta T}$ (CD45.2^{+}) plus *Brd7*$^{fl/fl}$ (CD45.1^{+}CD45.2^{+}) (n=3) at a ratio of 1:1. Chimeras were infected with HKx31 at 6 weeks after reconstitution, and sacrificed at 10 d p.i. for analysis. (**J-M**) Flow cytometry of OT-I CD8^{+} T cells (**J**) or KLRG1^{+}CD127^{-} SLECs and KLRG1^{-}CD127^{+} MEPCs (**L**) in CD45.1 host mice (n=4) 9 d after transfer of *Brd7*$^{fl/fl}$ (CD45.1^{+}CD45.2^{+}) plus *Brd7*$^{\Delta T}$ (CD45.2^{+}) OTI CD8^{+} T cells at a ratio of 1:1 and infection with PR8-OVA virus 1d after transfer. Small horizontal lines indicate the mean (± s.e.m.). **P*<0.05, ***P*<0.01 and ****P*<0.001 (two-tailed student *t* test). Data are representative of three independent experiments.

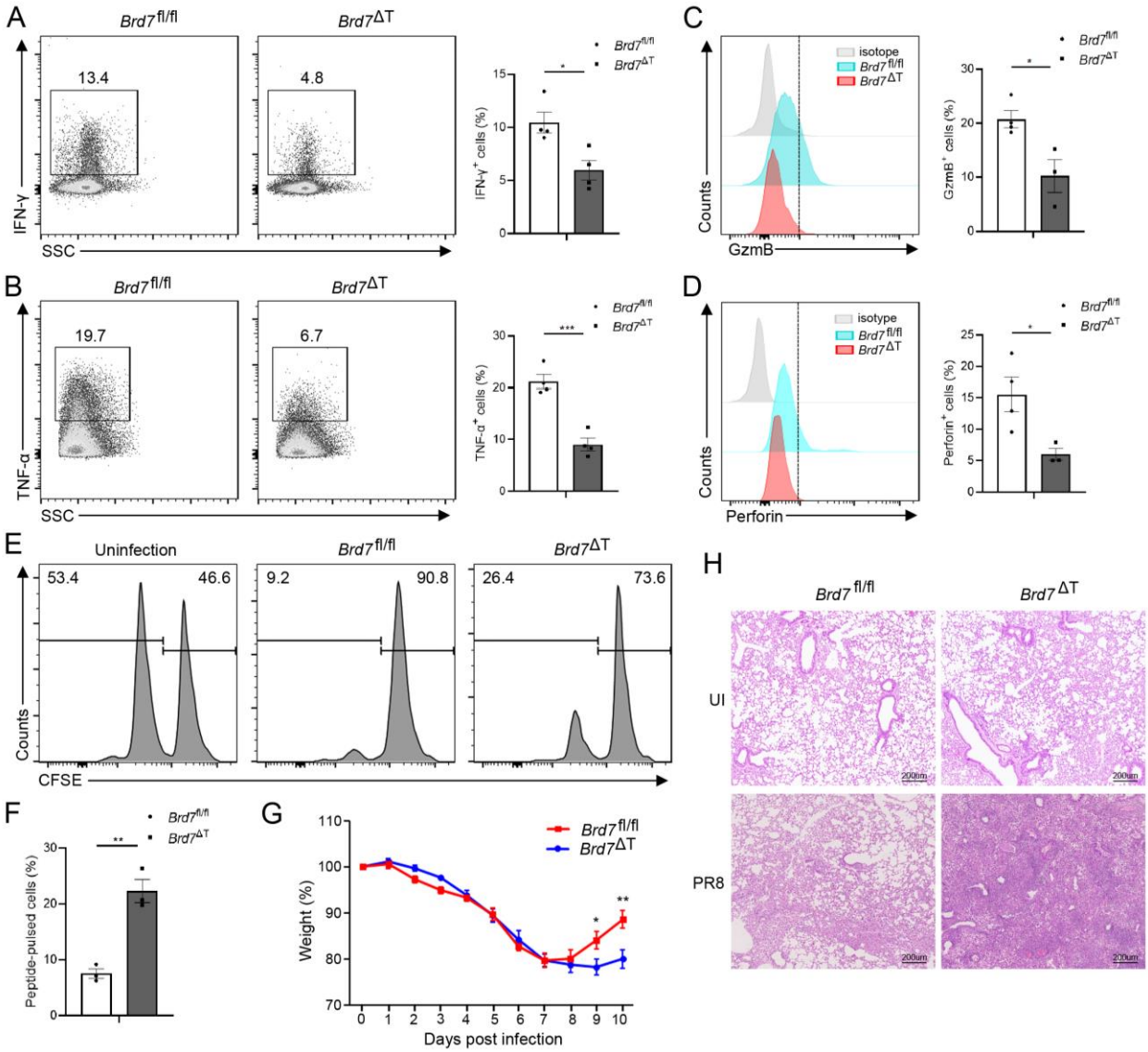
A
Brd7fl/fl
Brd7ΔT
13.4
4.8
IFN-γ
SSC
IFN-γ+ cells (%)
B
19.7
6.7
TNF-α
TNF-α+ cells (%)
C
isotope
Counts
GzmB
GzmB+ cells (%)
D
Perforin
Perforin+ cells (%)
E
Uninfection
53.4
46.6
9.2
90.8
26.4
73.6
CFSE
F
Peptide-pulsed cells (%)
G
Weight (%)
Days post infection
H
UI
PR8
200um

Figure 3

FIGURE 3. BRD7 is required for effector function. (**A-B**) Intracellular cytokine staining of IFN-γ (**A**) or TNF-α (**B**) produced by splenic $CD8^+$ T cells from *Brd7*$^{fl/fl}$ (n=4) and *Brd7*$^{\Delta T}$ (n=4) mice infected with HKx31 virus stimulated with NP peptide at 10 d p.i.. Left: Number in beside outlined areas indicates percent of IFN-γ^+CD8^+ (**A**) or TNF-α^+CD8^+ (**B**) T cells. Right: Frequency of IFN-γ^+ (**A**) or TNF-α^+ (**B**) cells among $CD8^+$ T cells in left. (**C-D**) Flow cytometry of granzyme B (GzmB) (**C**) or perforin (Prf1) (**D**) produced by splenic NP^+CD8^+ T cells from *Brd7*$^{fl/fl}$ (n=4) and *Brd7*$^{\Delta T}$ (n=3) mice infected with HKx31 virus at 10 d p.i.. Left: Numbers in beside outlined areas indicate Mean Fluorescence Intensity (MFI) of GzmB (**C**) or Prf1 (**D**) among NP^+CD8^+ T cells. Right: MFI of GzmB (**C**) or Prf1 (**D**) among NP^+CD8^+ T cells in left. (**E**) *In vivo* cytolysis assay. Non-infected wild-type host mice or infected BRD7-wild-type (n=3) or BRD7-deficient (n=3) mice received equal numbers of low CFSE-labeled B6 splenocytes loaded with NP peptide plus high CFSE-labeled B6 splenocytes without NP peptide stimulation at 10 d p.i.. Cytotoxic T lymphocyte activity was assessed 4 h after transfer. Numbers above bracketed lines represent percentages of cells per CFSE peak. (**F**) Frequency of peptide-pulsed cells in **E** was shown. (**G**) Body weight of *Brd7*$^{fl/fl}$ (n=8) and *Brd7*$^{\Delta T}$ (n=7) mice infected with 0.5 LD_{50} of A/PR/8/34 (H1N1) virus at various times p.i.. Body weight at day 0 was set as 100%. (**H**) Histological examination of lung from *Brd7*$^{fl/fl}$ or *Brd7*$^{\Delta T}$ mice non-infected with PR8 virus (top panel) or infected at 8 day p.i. (bottom panel). Lung from *Brd7*$^{\Delta T}$ mice infected with PR8 virus showed severe tissue damage and lymphocytic infiltration. Small horizontal lines indicate the mean (± s.e.m.). **P*<0.05, ***P*<0.01 and ****P*<0.001 (two-tailed student *t* test). Data are representative of three independent experiments.

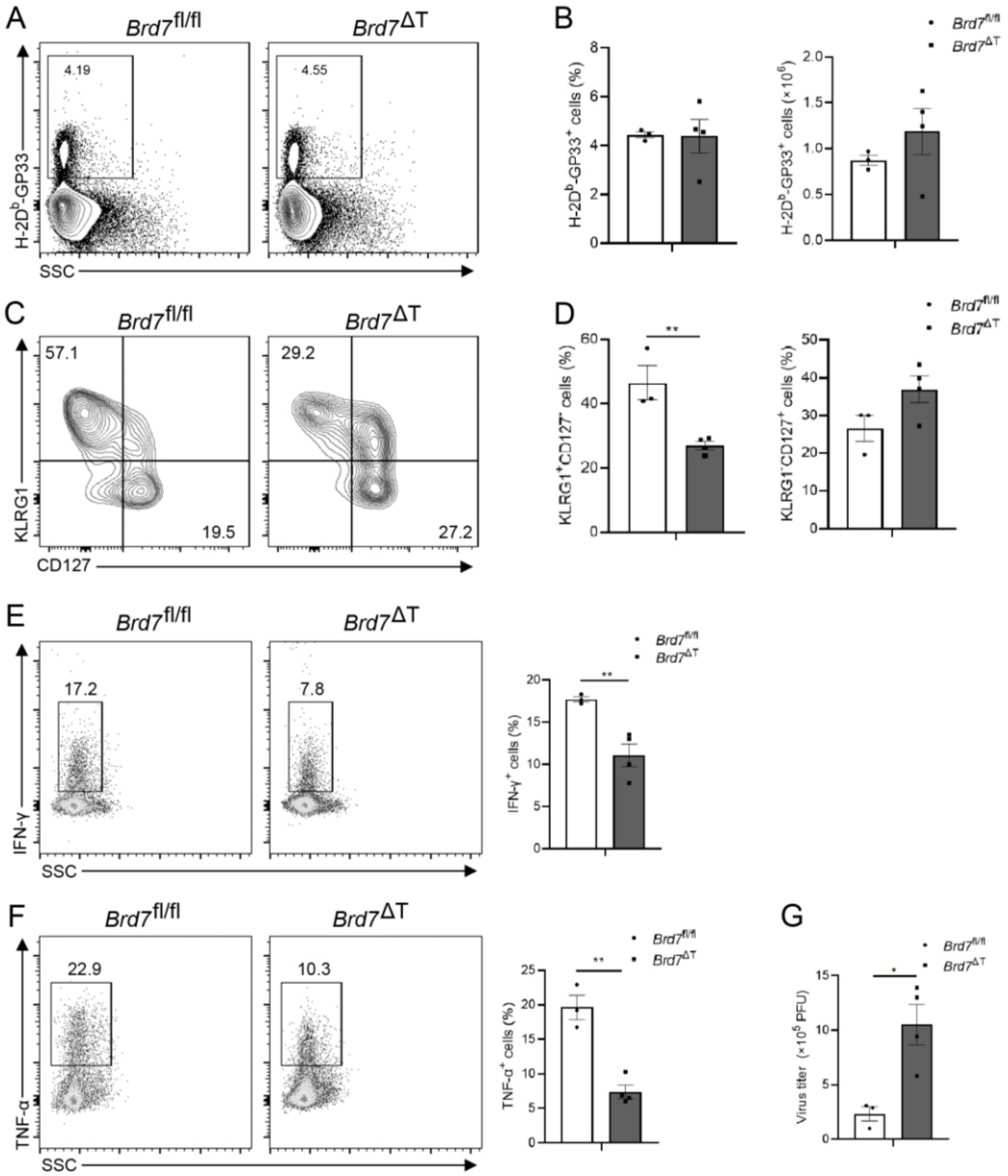
A
Brd7fl/fl
Brd7ΔT
4.19
4.55
H-2Db-GP33
SSC
B
Brd7fl/fl
Brd7ΔT
H-2Db-GP33+ cells (%)
H-2Db-GP33+ cells (×10^6)
C
Brd7fl/fl
Brd7ΔT
57.1
29.2
19.5
27.2
KLRG1
CD127
D
Brd7fl/fl
Brd7ΔT
**
KLRG1+CD127- cells (%)
KLRG1-CD127+ cells (%)
E
Brd7fl/fl
Brd7ΔT
17.2
7.8
IFN-γ
SSC
**
IFN-γ+ cells (%)
F
Brd7fl/fl
Brd7ΔT
22.9
10.3
TNF-α
SSC
**
TNF-α+ cells (%)
G
Brd7fl/fl
Brd7ΔT
*
Virus titer (×10^5 PFU)

Figure 4

FIGURE 4. BRD7 controls SLEC differentiation during LCMV infection. (**A**) Flow cytometry of Arm gp33^{+}CD8^{+} T cells from spleen of *Brd7*$^{fl/fl}$ (n=3) and *Brd7*$^{\Delta T}$ (n=4) mice. *Brd7*$^{fl/fl}$ and *Brd7*$^{\Delta T}$ mice were infected with LCMV armstrong virus, and antigen-specific gp33 tetramer was stained in spleen CD8^{+} T cells at 8 d p.i.. Numbers in beside outlined areas indicate percent of gp33^{+}CD8^{+} T cells. (**B**) Frequency (left) and cell number (right) of gp33-specific cells among CD8^{+} T cells in **A**. (**C**) Flow cytometry of KLRG1 and CD127 on gp33^{+}CD8^{+} T cells in the spleen obtained from *Brd7*$^{fl/fl}$ (n=3) or *Brd7*$^{\Delta T}$ (n=4) mice infected with Arm at 8 d p.i.. Numbers in quadrants indicate percent of KLRG1^{+}CD127^{-} SLECs (top left) or KLRG1^{-}CD127^{+} MEPCs (bottom right). (**D**) Frequency of KLRG1^{+}CD127^{-} SLECs or KLRG1^{-}CD127^{+} MEPCs among gp33^{+}CD8^{+} T cells in **C**. (**E-F**) Intracellular cytokine staining of IFN-γ (**E**) or TNF-α (**F**) produced by splenic CD8^{+} T cells from *Brd7*$^{fl/fl}$ (n=3) and *Brd7*$^{\Delta T}$ (n=4) mice infected with Arm virus stimulated with gp33 peptide at 8 d p.i.. Left: Number in beside outlined areas indicate percent of IFN-γ^{+}CD8^{+} (**E**) or TNF-α^{+}CD8^{+} (**F**) T cells. Right: Frequency of IFN-γ^{+} (**E**) or TNF-α^{+} (**F**) cells among CD8+ T cells in left. (**G**) LCMV arm virus titers in the spleen of *Brd7*$^{fl/fl}$ (n=3) or *Brd7*$^{\Delta T}$ (n=4) mice infected with LCMV arm strain were determined at day 8 p.i.. Small horizontal lines indicate the mean (± s.e.m.). **P*<0.05, ***P*<0.01 and ****P*<0.001 (two-tailed student *t* test). Data are representative of three independent experiments.

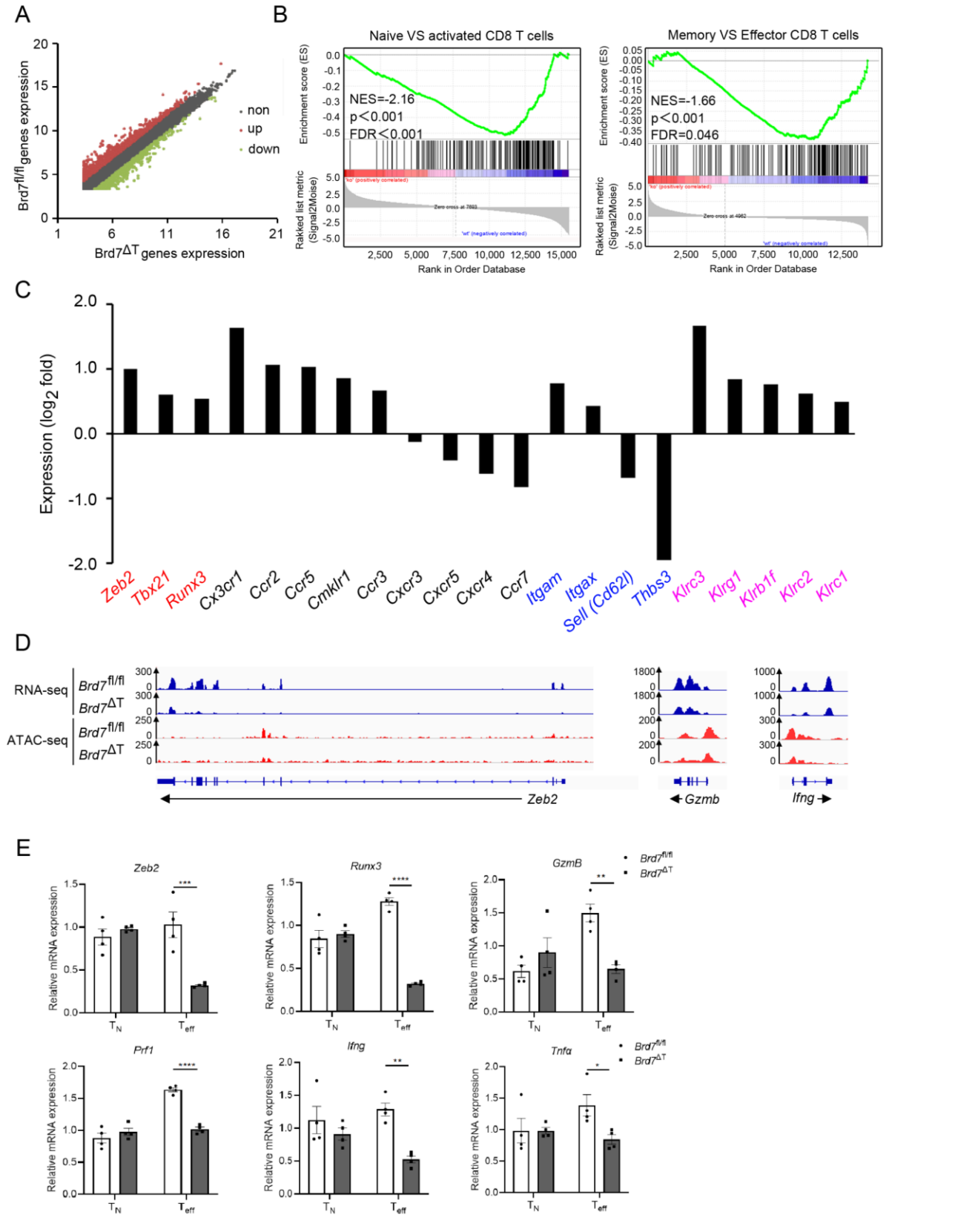
A
Brd7fl/fl genes expression
Brd7ΔT genes expression
non
up
down
B
Naive VS activated CD8 T cells
NES=-2.16
p<0.001
FDR<0.001
Memory VS Effector CD8 T cells
NES=-1.66
p<0.001
FDR=0.046
Enrichment score (ES)
Rakked list metric (Signal2Moise)
Rank in Order Database
C
Expression (log2 fold)
Zeb2
Tbx21
Runx3
Cx3cr1
Ccr2
Ccr5
Cmklr1
Ccr3
Cxcr3
Cxcr5
Cxcr4
Ccr7
Itgam
Itgax
Sell (Cd62l)
Thbs3
Klrc3
Klrg1
Klrb1f
Klrc2
Klrc1
D
RNA-seq
ATAC-seq
Brd7fl/fl
Brd7ΔT
Zeb2
Gzmb
Ifng
E
Zeb2
Runx3
GzmB
Prf1
Ifng
Tnfα
Relative mRNA expression
TN
Teff
Brd7fl/fl
Brd7ΔT

Figure 5

FIGURE 5. BRD7 orchestrates the expression of genes critical for SLEC differentiation. (**A**) Scatter plot analysis of differentially expressed genes of NP^+ $CD8^+$ T cells from *Brd7*$^{fl/fl}$ and *Brd7*$^{\Delta T}$ mice infected with HKx31 at 10 d p.i. FDR ≤ 0.05 and Log 2 FC ≥ 2 were used as the threshold to evaluate the significance of differences in gene expression. (**B**) Gene set enrichment analysis (GSEA) in **A** among transcriptional differences between naïve and activated $CD8^+$ T cells (left) or memory and effector cells (right). NES, normalized enrichment score. FDR, false discovery rate; (**C**) Differentially expressed genes of transcription factor (red), chemokine receptors (black), adhesion molecules (blue), and killer cell lectin-like receptors (pink) between wild-type and BRD7-deficient cells, represented as the log2 fold change. The y-axis displays the -log2 fold change of each DEG and the x-axis lists the gene name. (**D**) Genome browser tracks displaying RNA-seq and ATAC-seq data at a selected locus comparing wild-type and BRD7-deficient cells. Tag density from different groups was calculated by normalizing to the total mapped reads. (**E**) Quantitative PCR analysis of mRNA in BRD7-deficient naïve $CD8^+$ T cells (T_N) or NP^+CD8^+ T cells (T_{eff}) (n=4) presented relative to expression in BRD7-wild-type cells (n=4). Small horizontal lines indicate the mean (± s.e.m.). **P*<0.05, ***P*<0.01 and ****P*<0.001 (two-tailed student *t* test). Data are representative of two independent experiments.

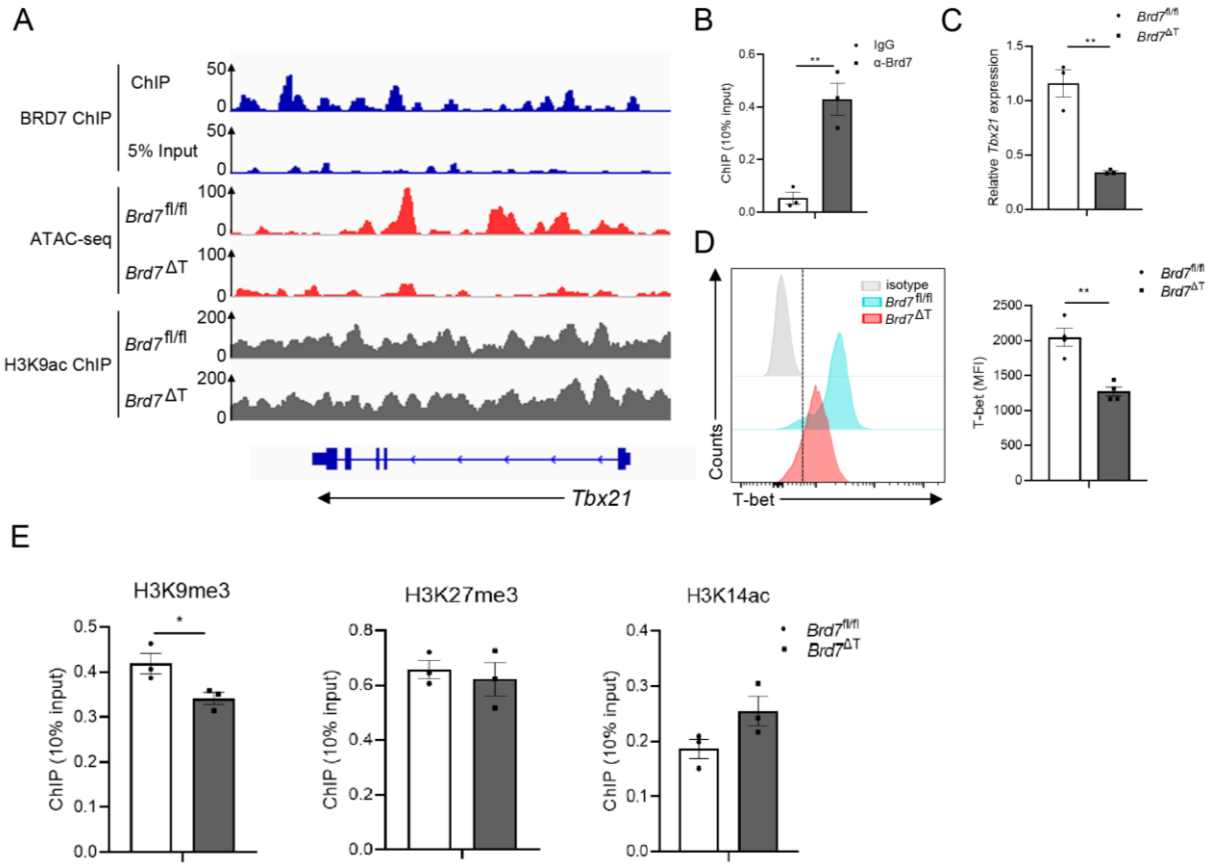
A
BRD7 ChIP
ChIP
5% Input
ATAC-seq
Brd7fl/fl
Brd7ΔT
H3K9ac ChIP
Tbx21
B
IgG
α-Brd7
ChIP (10% input)
C
Relative Tbx21 expression
D
isotype
Counts
T-bet
T-bet (MFI)
E
H3K9me3
H3K27me3
H3K14ac
ChIP (10% input)

Figure 6

FIGURE 6. BRD7 is enriched at *Tbx21* loci and regulates T-bet expression. (**A**) Representative alignments of ChIP-, ATAC- and RNA-seq measurements at *Tbx21* loci. ATAC- and RNA-seq measurements from cells in Figure 5. ChIP-seq with antibody to BRD7 was assessed with OT-I $CD8^+$ T cells from OT-I mice infected with PR8-OVA at day 8 p.i.. ChIP-seq with antibody to H3K9ac was assessed with OT-I $CD8^+$ T cells from *Brd7*$^{fl/fl}$ and *Brd7*$^{\Delta T}$ OT-I mice infected with PR8-OVA at day 8 p.i.. (**B**) ChIP analysis (n=3) shows the deposition of BRD7 at the promoter regions of *Tbx21* loci. (**C**) Quantitative PCR analysis of *T-bet* mRNA in BRD7-deficient NP^+CD8^+ T cells (n=3) presented relative to expression in BRD7-wild-type cells (n=3). (**D**) Left: flow cytometry of T-bet in BRD7-wild-type (n=4) or BRD7-deficient (n=4) NP^+CD8^+ T cells. Right: frequency of T-bet expressing NP^+CD8^+ T cells in left. (**E**) ChIP-PCR assay shows the deposition of H3K9me3, H3K27me3, and H3K14ac at the promoter regions of *Tbx21* loci. *Brd7*$^{fl/fl}$ mice (n=3) and *Brd7*$^{\Delta T}$ mice (n=3) were used in the experiments. Small horizontal lines indicate the mean (± s.e.m.). **P*<0.05, ***P*<0.01 and ****P*<0.001 (two-tailed student *t* test). Data are representative of two independent experiments.

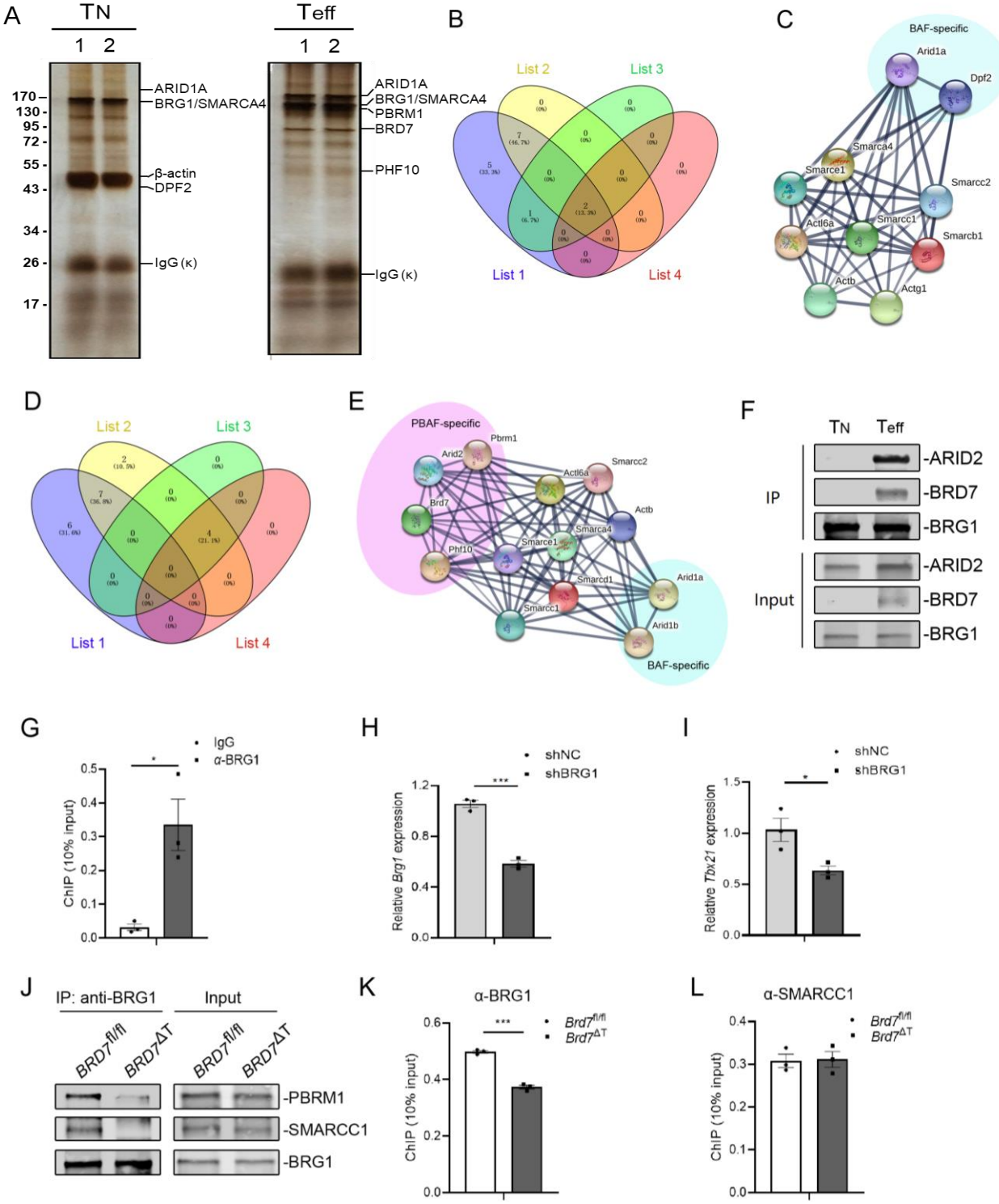
A
TN
Teff
1 2
1 2
170
130
95
72
55
43
34
26
17
ARID1A
BRG1/SMARCA4
β-actin
DPF2
IgG (κ)
ARID1A
BRG1/SMARCA4
PBRM1
BRD7
PHF10
IgG (κ)
B
List 2
List 3
List 1
List 4
C
BAF-specific
Arid1a
Dpf2
Smarca4
Smarce1
Smarcc2
Actl6a
Smarcc1
Smarcb1
Actb
Actg1
D
List 2
List 3
List 1
List 4
E
PBAF-specific
Pbrm1
Arid2
Smarcc2
Actl6a
Brd7
Actb
Smarca4
Smarce1
Phf10
Smarcd1
Arid1a
Smarcc1
Arid1b
BAF-specific
F
TN
Teff
IP
-ARID2
-BRD7
-BRG1
Input
-ARID2
-BRD7
-BRG1
G
IgG
α-BRG1
ChIP (10% input)
H
shNC
shBRG1
Relative Brg1 expression
I
shNC
shBRG1
Relative Tbx21 expression
J
IP: anti-BRG1
Input
BRD7fl/fl
BRD7ΔT
BRD7fl/fl
BRD7ΔT
-PBRM1
-SMARCC1
-BRG1
K
α-BRG1
Brd7fl/fl
Brd7ΔT
ChIP (10% input)
L
α-SMARCC1
Brd7fl/fl
Brd7ΔT
ChIP (10% input)

Figure 7

FIGURE 7. BRD7 functions as a bridge for PBAF complex to efficiently assembly in effector CD8$^+$ T cells. (**A**) Mass spectrum analysis of BRG1-associated proteins in naïve OT-I CD8$^+$ T (n=2) or effector OT-I CD8$^+$ T cells (n=2) from OT-I mice infected with PR8-OVA at day 8 p.i.. (**B**) Venn diagram showing the overlap of components. List 1: Reported-components of BAF complex. List 2: Identified components of BAF complex from naïve cells in **A**. List 3: Reported BAF-specific components. List 4: Identified BAF-specific from naïve cells in **A**. (**C**) SWI/SNF components from naïve T cells in **A** were clustered with STRING analysis. (**D**) Venn diagram showing the overlap of components. List 1: Reported-components of PBAF complex. List 2: Identified components of PBAF complex from effector cells in **A**. List 3: Reported PBAF-specific components. List 4: Identified PBAF-specific from effector cells in **A**. (**E**) SWI/SNF components from effector cells in **A** were clustered with STRING analysis. (**F**) Co-IP of BRG1-associated proteins in naïve CD8$^+$ T (n=2) or effector CD8$^+$ T cells (n=2) from OT-I mice infected with PR8-OVA. (**G**) ChIP (n=3) shows the deposition of BRG1 at the promoter regions of *Tbx21* loci. (**H-I**) The mRNA expression (n=3) of *Brg1* and *Tbx21* of OT-I T cells of shRNA was analyzed at 8 day after transfer into recipient mice infected with PR8-OVA virus. (**J**) Co-IP of BRG1 in BRD7-wild-type and BRD7-deficient CD8$^+$ T cells from OT-I mice infected with PR8-OVA at day 8 p.i.. (**K-L**) ChIP (n=3) shows the deposition of BRG1 and SMARCC1 at the promoter of *Tbx21* in BRD7-wild-type and BRD7-deficient CD8$^+$ T cells from OT-I mice infected with PR8-OVA at day 8 p.i.. Small horizontal lines indicate the mean (± s.e.m.). *P<0.05, **P<0.01 and ***P<0.001 (two-tailed student t test). Data are representative of two independent experiments.